Master Thesis

Technische Universität Wien
Institute of Telecommunications

Emulation Techniques for High Speed Train Measurements in 6G Mobile Communications

Faruk Pasic, B.Sc.
student number: 11802515

Supervision:
Univ. Prof. Dipl.-Ing. Dr.techn. Markus Rupp
Projektass. B.Sc. Dipl.-Ing. Dr.techn. Stefan Pratschner

Die approbierte gedruckte Originalversion dieser Diplomarbeit ist an der TU Wien Bibliothek verfügbar
The approved original version of this thesis is available in print at TU Wien Bibliothek.

Die approbierte gedruckte Originalversion dieser Diplomarbeit ist an der TU Wien Bibliothek verfügbar
The approved original version of this thesis is available in print at TU Wien Bibliothek.

Statement on Academic Integrity

I hereby declare and confirm with my signature that the doctoral dissertation is exclusively the result of my own autonomous work, based on my research and literature published, which is seen in the notes and bibliography used. I also declare that no part submitted has been made in an inappropriate way, whether by plagiarizing or infringing on any third person's copyright. Finally, I declare that no part submitted has been plagiarized for any other paper in another higher education institution, research institution or educational institution.

Vienna, July 2021

Author's signature

Supervisor's signature

Die approbierte gedruckte Originalversion dieser Diplomarbeit ist an der TU Wien Bibliothek verfügbar
The approved original version of this thesis is available in print at TU Wien Bibliothek.
TU Bibliothek Your knowledge hub WIEN

Die approbierte gedruckte Originalversion dieser Diplomarbeit ist an der TU Wien Bibliothek verfügbar
The approved original version of this thesis is available in print at TU Wien Bibliothek.

Abstract

High-speed train (HST) scenarios are expected to be typical scenarios for sixth-generation (6G) wireless communication systems. Due to the high cost, complexity, and time consumption of high-speed measurement campaigns, this particular environment poses challenges for performance measurements. Furthermore, it is not possible to perform repeatable measurements in a controlled high-speed environment in most cases. Using proposed methods of time-stretching the transmit signals, fortunately, such experiments can be emulated at lower velocities by inducing effects caused by highly time-varying channels. Therefore, the cost and complexity of high-speed measurement campaigns are considerably decreased. Foremost, this thesis considers the problem of unequal channel estimation quality between proposed time-stretching methods. This is an auxiliary unwanted side effect of proposed time-stretching methods. To ensure a fair comparison between resampling- and insertion-based time-stretching methods, I adapt the pilot-based channel estimation scheme within the time-stretching method. Besides the unequal channel estimation quality, I consider the problem of significantly increased Peak-to-Average Power Ratio (PAPR) in time-stretching methods. To solve this problem, I apply strategies to reduce the PAPR. Thereby, time-stretching methods can be used more efficiently in practical communication systems. In addition, this thesis investigates the applicability of the proposed time-stretching methods for 6G candidate waveforms. Evaluation is performed by simulations in high-speed environment scenarios. More specifically, I compare the performance of proposed methods by employing waveform candidates proposed for 6G wireless communication systems, such as Orthogonal Frequency Division Multiplexing (OFDM), Filter Bank Multi-carrier (FBMC), and Universal Filtered Multi-carrier (UFMC).

Die approbierte gedruckte Originalversion dieser Diplomarbeit ist an der TU Wien Bibliothek verfügbar
The approved original version of this thesis is available in print at TU Wien Bibliothek.
TU Bibliothek Your knowledge hub WIEN

Die approbierte gedruckte Originalversion dieser Diplomarbeit ist an der TU Wien Bibliothek verfügbar
The approved original version of this thesis is available in print at TU Wien Bibliothek.

Kurzfassung

Kommunikationsszenarien mit Hochgeschwindigkeitszügen sind ein typischer Bestandteil drahtloser Kommunikation der 6ten Generation. Aufgrund der hohen Kosten, Komplexität und des Zeitaufwands von Messkampangnen bei hoher Geschwindigkeit stellt diese spezielle Umgebung Performance Messungen vor große Herausforderungen. Darüber hinaus ist es in den meisten Fällen nicht möglich, wiederholbare Messungen in einer kontrollierten Hochgeschwindigkeitsumgebung durchzuführen. Glücklicherweise können solche Experimente unter Anwendung von Time-Stretching-Methoden der Sendesignale bei niedrigeren Geschwindigkeiten emuliert werden. Damit werden Effekte, die durch stark zeitselektiv Kanäle verursacht werden, induziert. Daher werden die Kosten und die Komplexität von Messkampangnen bei hoher Geschwindigkeit erheblich verringert. Erstens betrachtet diese Arbeit das Problem der ungleichen Kanalschätzungsqualität zwischen den vorgeschlagenen Time-Stretching-Methoden. Dies ist ein unerwünschter Nebeneffekt der vorgeschlagenen Zeitdehnungsverfahren. Um einen fairen Vergleich zwischen Time-Stretching-Verfahren zu gewährleisten, passe ich das pilotbasierte Kanalschätzungsschema innerhalb des Time-Stretching-Verfahrens an. Neben der ungleichen Kanalschätzungsqualität betrachte ich das Problem des deutlich erhöhten Peak-to-Average Power Ratio (PAPR) bei Time-Stretching-Verfahren. Um dieses Problem zu lösen, wende ich bekannte Strategien aus der Literatur zur Reduzierung des PAPR an. Dadurch können Time-Stretching-Verfahren in praktischen Kommunikationssystemen effizienter verwendet werden. Außerdem untersucht diese Arbeit die Anwendbarkeit der vorgeschlagenen Time-Stretching-Methoden für 6G-Mehrträgermodulation Formate. Die Auswertung erfolgt durch Simulationen in Hochgeschwindigkeitsumgebungsszenarien. Genauer gesagt vergleiche ich Modulationsverfahren durch Verwendung von Wellenformkandidaten, die für drahtlose 6G-Kommunikationssysteme vorgeschlagen wurden, wie z. B. Orthogonal Frequency Division Multiplexing (OFDM), Filter Bank Multi-Carrier (FBMC) und Universal Filtered Multi-Carrier (UFMC) im Bezug auf die Anwendung von Time-Stretching-Methoden.

Die approbierte gedruckte Originalversion dieser Diplomarbeit ist an der TU Wien Bibliothek verfügbar
The approved original version of this thesis is available in print at TU Wien Bibliothek.
TU Bibliothek Your knowledge hub WIEN

Die approbierte gedruckte Originalversion dieser Diplomarbeit ist an der TU Wien Bibliothek verfügbar
The approved original version of this thesis is available in print at TU Wien Bibliothek.

Table of Abbreviations

3G	Third Generation
4G	Fourth Generation
5G	Fifth Generation
AWGN	Additive White Gaussian Noise
BER	Bit Error Rate
CP	Cyclic Prefix
CSI	Channel State Information
DFT	Discrete Fourier Transform
FBMC	Discrete Fourier Transform
FDM	Frequency-Division Multiplexing
FIR	Finite Impulse Response
FFT	Fast Fourier Transform
GSM	Global System for Mobile Communications
ICI	Intercarrier Interference
IDFT	Inverse Discrete Fourier Transform
IFFT	Inverse Fast Fourier Transform
ISI	Intersymbol Interference
LTE	Long-Term Evolution
MSE	Mean Squared Error
OFDM	Orthogonal Frequency-Division Multiplexing
OOB	Out-of-Band
OQAM	Offset Quadrature Amplitude Modulation
PA	Power Amplifier

Die approbierte gedruckte Originalversion dieser Diplomarbeit ist an der TU Wien Bibliothek verfügbar
The approved original version of this thesis is available in print at TU Wien Bibliothek.
TU Bibliothek Your knowledge hub WIEN

PAM	Pulse Amplitude Modulation
PAPR	Peak-to-Average Power Ratio
PSD	Power Spectral Density
QAM	Quadrature Amplitude Modulation
SIR	Signal-to-Interference Ratio
SNR	Signal-to-Noise Ratio
UFMC	Universal Filtered Multicarrier

Die approbierte gedruckte Originalversion dieser Diplomarbeit ist an der TU Wien Bibliothek verfügbar
The approved original version of this thesis is available in print at TU Wien Bibliothek.
TU Bibliothek Your knowledge hub WIEN

Contents

Die approbierte gedruckte Originalversion dieser Diplomarbeit ist an der TU Wien Bibliothek verfügbar
The approved original version of this thesis is available in print at TU Wien Bibliothek.
TU Bibliothek Your knowledge hub WIEN

Die approbierte gedruckte Originalversion dieser Diplomarbeit ist an der TU Wien Bibliothek verfügbar
The approved original version of this thesis is available in print at TU Wien Bibliothek.

1 Outline

This thesis considers the problem of performing mobile communications measurements with the experimental user equipment in a high-speed train scenario.

Section 2 introduces the problem of performing channel measurements in a high-speed environment and explains why such measurements are very challenging and sometimes even impossible to perform. This section also outlines a possible solution to this problem by using emulation techniques to induce effects of high-speed train (HST) channel while conducting measurements at much lower speeds.

In Section 3, I explain the principle of already proposed methods to emulate higher velocities by conducting measurements at lower velocities. I also show the main differences between the two emulation methods. One of them is based on resampling and repeating the same signal, while the other is based on the insertion of additional subcarriers between data subcarriers.

In Section 4, I adapt the pilot-based channel estimation scheme within resampling- and insertion-based time-interpolation methods. Thus, the channel estimation error is then equal to the system without an interpolation method applied.

In Section 5, I adapt Peak-to-Average Power Ratio (PAPR) reduction methods within time-interpolation methods, such that they can be used in practical communication systems more efficiently.

Section 6 provides a detailed comparative overview of multi-carrier schemes proposed for use in 6G systems, with the aim of using them in time-stretching methods. Multi-carrier schemes considered in this section are Filter Bank Multi-carrier (FBMC) and Universal Filtered Multi-carrier (UFMC).

In Section 7, I provide a more general simulation study in terms of the Signal-to-Interference Ratio (SIR) and the physical layer throughput. Firstly, I show how adapted channel estimation scheme and PAPR reduction methods impact the throughput of a transmission system. Thereafter, I apply interpolation methods on Filter Bank Multi-carrier (FBMC) and Universal Filtered Multi-carrier (UFMC) schemes and evaluate their emulation performance.

Die approbierte gedruckte Originalversion dieser Diplomarbeit ist an der TU Wien Bibliothek verfügbar
The approved original version of this thesis is available in print at TU Wien Bibliothek.
TU Bibliothek Your knowledge hub WIEN

Die approbierte gedruckte Originalversion dieser Diplomarbeit ist an der TU Wien Bibliothek verfügbar
The approved original version of this thesis is available in print at TU Wien Bibliothek.

2 Introduction

High-speed railway (HSR) is generally considered as one of the most sustainable developments for ground transportation. Compared with conventional ground transportation systems, HSR offers higher mobility and lower environmental impact. In the future, there will be more advances in railway systems to improve the quality and the safety of rail services. The rail traffic is expected to evolve into a new era of "smart rail mobility" where infrastructure, trains, travelers, and goods will be increasingly interconnected [1]. Apart from handling critical signaling applications, the railway architecture will include various services to enable intelligent traffic management such as fully automatic train operation, real-time monitoring, and journey information [2]. Nevertheless, upcoming new railway technologies are also expected to offer passengers various services such as Internet access and high-quality voice or mobile video broadcasting [3]. Such services require a communication system that can provide high data rates in high-mobility scenarios.

Existing railway communication systems are based on Global system for mobile communications for Railway (GSM-R) and Long-term evolution for Railway (LTE-R). Actually, GSM-R and LTE-R represent GSM and LTE, respectively, with specific railway functionalities. Unfortunately, these communication systems cannot meet high data rate requirements in an HSR environment. These systems are designed for users with low or medium mobility. High mobility scenarios with speeds of up to 500 km/h significantly limit their coverage area and transmission rate [4].

To effectively support the design and development of the communication systems for railways, it is essential to perform channel measurements in high-speed scenarios. So far, few measurements in such an environment were conducted by employing LTE signals. Unterhuber et al. [5] focused on the wideband propagation for train-to-train (T2T) scenarios and described an extensive channel-sounding measurement campaign with two high-speed trains (HST). Apart from T2T scenarios, Rodríguez-Piñeiro et al. [6] measured characteristics of the wireless channel between a base-station transmitter and a mobile receiver with antennas placed on the top of a high-speed train. In [7] and [8], authors presented analysis and measurements of MIMO channel in an HSR environment.

Measurements in HST scenarios were also conducted at mmWave frequencies. Authors of [9] and [1] presented HST measurement campaigns investigating channel characteristics of a rural environment and tunnel scenario, respectively. Park et al. [10] investigated mmWave propagation characteristics of a high-speed moving train based on field measurements in both tunnel and viaduct scenarios.

Die approbierte gedruckte Originalversion dieser Diplomarbeit ist an der TU Wien Bibliothek verfügbar
The approved original version of this thesis is available in print at TU Wien Bibliothek.
TU Bibliothek Your knowledge hub WIEN

Performing mobile communications measurements with an experimental user equipment in an HST environment is very challenging since it is expensive, time-consuming, and complex. Due to high speeds, sometimes it can be dangerous or even impossible. This is one of the main reasons why only a small number of measurements have been performed in such an environment so far. Furthermore, it is hardly possible to perform the measurement at high speeds in a controlled environment and in a repeatable manner. The repeatability of results is basically lost because it is challenging to maintain identical environmental conditions and keep the train speed constant during the measurement. In addition, if any modification in a realistic measurement environment is made, it is impossible to ensure fair comparisons with future measurements. Consequently, researchers are often forced to test new techniques only through simulations.

As a possible solution, the authors of [11] proposed a technique to induce effects caused by highly time-varying channels in OFDM signals while conducting measurements at much lower speeds. The accuracy of the proposed technique has been experimentally evaluated in [12] and [13] by employing a setup that allows for repeatable measurements at different speeds up to 200 km/h in a controlled measurement environment. Nevertheless, Lerch et al. [14] proposed a set of new techniques to induce such effects by stretching OFDM signals in a different way.

In [14], there is an auxiliary unwanted channel estimation side effect of resampling-based time-stretching techniques. More precisely, resampling of the original signal increases or decreases pilot spacing in the frequency-domain. Therefore, it leads to unequal channel estimation quality between resampling- and insertion-based time-stretching techniques. Consequently, without knowing the channel state information (CSI) at the receiver, proposed time-stretching techniques can not be compared in a fair manner. To ensure a fair comparison between resampling- and insertion-based time-stretching techniques, I adapt the pilot-based channel estimation scheme within the resampling-based time-stretching technique.

One more issue that arises when employing time-stretching techniques to emulate highly time-varying channels is a significant increase in PAPR. For all proposed time-stretching techniques, it occurs due to an increased number of subcarriers. For the resampling-based time-stretching technique, PAPR is additionally increased, since the same signal is repeated more times. Increased PAPR limits the choice of a power amplifier at the transmitter, which results in degradation of whole system performance, including the SNR at the receiver. On the other hand, if increased PAPR is neglected, it can cause a gain compression, spectral growth, and out-of-band radiation of the multi-carrier signal. To solve this problem, I adapt already proposed Peak-to-Average

Die approbierte gedruckte Originalversion dieser Diplomarbeit ist an der TU Wien Bibliothek verfügbar
The approved original version of this thesis is available in print at TU Wien Bibliothek.
TU Bibliothek Your knowledge hub WIEN

Power Ratio (PAPR) reduction methods within time-interpolation techniques, such that they can be used with more efficient power amplifiers in practical communication systems.

In [14], the validation of new techniques to induce effects caused by highly time-varying channels while conducting measurements at much lower speeds is performed on OFDM waveform only. The OFDM waveform poses a reduced spectral efficiency, stringent synchronization requirement, and poor performance in doubly selective HST channels. Therefore, it is essential to find other communication technologies that can cope with the challenges and difficulties of HSR scenarios. Fortunately, a possible solution lies in the sixth-generation (6G) wireless communication system. Using filter-based waveform candidates, such as Filter Bank Multi-carrier (FBMC) and Universal Filtered Multi-carrier (UFMC), 6G systems tend to increase the spectral efficiency and the performance in doubly selective channels. Therefore, I validate the performance of time-stretching methods proposed in [11] and [14] through FBMC and UFMC waveforms.

Die approbierte gedruckte Originalversion dieser Diplomarbeit ist an der TU Wien Bibliothek verfügbar
The approved original version of this thesis is available in print at TU Wien Bibliothek.
TU Bibliothek Your knowledge hub WIEN

Die approbierte gedruckte Originalversion dieser Diplomarbeit ist an der TU Wien Bibliothek verfügbar
The approved original version of this thesis is available in print at TU Wien Bibliothek.

3 Interpolation Methods

In this section, I explain the principle of methods to emulate higher velocities by conducting measurements at lower velocities, proposed in [14]. I also show the main differences between two emulation methods, "Resample & Repeat" based on resampling and repeating the same signal, and "Random Symbols" based on the insertion of additional subcarriers between data subcarriers.

3.1 Introduction to interpolation methods

High-velocity emulation methods are designed for digital multi-carrier modulation techniques. To understand its principle of work, it is first necessary to explain the basics of the multi-carrier modulation technique. The most widely used multi-carrier technique is Orthogonal Frequency Division Multiplexing (OFDM). OFDM is a special case of digital multi-carrier modulation technique proposed by Chang [15] in 1966. The concept of OFDM is based on Frequency Division Multiplexing (FDM), in which a wideband transmit channel is divided into multiple spectrally overlapping subchannels. Each subchannel is modulated separately, and then several subchannels are frequency multiplexed. To avoid a cross-talk between subcarriers due to the overlapping, they need to be mutually orthogonal.

Let us consider an OFDM communication system represented in discrete-time domain matrix form [16]. The block diagram of such OFDM transceiver is shown in Figure 3.1. A block of N symbols modulated by Quadrature Amplitude Modulation (QAM) is mapped onto N different subcarriers to construct an OFDM symbol. A single OFDM symbol is represented as vector $\mathbf{x} \in \mathbb{C}^{N\times 1}$, where

$$\mathbf{x} = \begin{bmatrix} \mathrm{x}_1 & \mathrm{x}_2 & \dots & \mathrm{x}_N \end{bmatrix}^{\mathsf{T}}. \tag{3.1}$$

The OFDM symbol passes the Inverse Discrete Fourier Transform (IDFT) block of size N_{FFT} for the transformation to the time domain. In order to increase the frequency resolution of the IDFT, $(N_{\mathrm{FFT}} - N)$ zeros are appended to the $\mathbf{x}$. Thereby, the modified OFDM symbol is represented as vector $\tilde{\mathbf{x}} \in \mathbb{C}^{N_{\mathrm{FFT}}\times 1}$, where

$$\tilde{\mathbf{x}} = \mathbf{A}_{N_{\mathrm{FFT}}}\mathbf{x}. \tag{3.2}$$

In (3.2), the $\mathbf{A}_{N_{\mathrm{FFT}}}$ is the $N_{\mathrm{FFT}} \times N$ matrix, given by

$$\mathbf{A}_{N_{\mathrm{FFT}}} = \begin{bmatrix} \mathbf{I}_N \\ \mathbf{0} \end{bmatrix}. \tag{3.3}$$

After that, the cyclic prefix (CP) is inserted by adding N_{CP} samples to the transformed OFDM symbol. The CP is a copy of the last part of the OFDM symbol, which is

Die approbierte gedruckte Originalversion dieser Diplomarbeit ist an der TU Wien Bibliothek verfügbar
The approved original version of this thesis is available in print at TU Wien Bibliothek.
TU Bibliothek Your knowledge hub WIEN

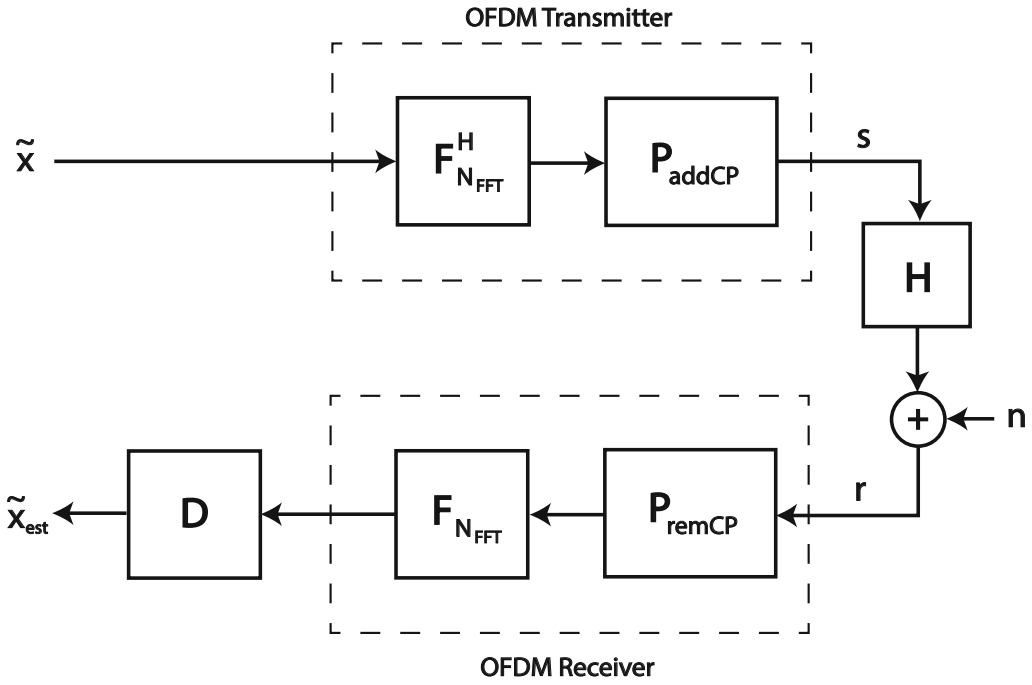

Figure 3.1: The OFDM divides a wideband transmit channel into multiple spectrally overlapping orthogonal subchannels.

prepended to the transmitted symbol in order to avoid intersymbol interference (ISI) from the previous symbol [17]. The transmit signal $\mathbf{s}$ is compactly formulated via matrix multiplications

$$\mathbf{s} = \mathbf{P}_{\text{addCP}} \mathbf{F}^{\text{H}}_{N_{\text{FFT}}} \mathbf{A}_{N_{\text{FFT}}} \mathbf{x} \tag{3.4}$$

where $\mathbf{F}^{\text{H}}_{N_{\text{FFT}}}$ is the standard $N_{\text{FFT}} \times N_{\text{FFT}}$ IDFT matrix and

$$\mathbf{P}_{\text{addCP}} = \begin{bmatrix} \mathbf{0} & \mathbf{I}_{N_{\text{CP}}} \\ & \mathbf{I}_{N_{\text{FFT}}} \end{bmatrix} \in \mathbb{R}^{(N_{\text{FFT}}+N_{\text{CP}}) \times N_{\text{FFT}}} \tag{3.5}$$

describes the addition of the CP of length N_{CP}. The transmit signal $\mathbf{s}$ is then transmitted over a multipath propagation channel with the channel impulse response (CIR) denoted by $\mathbf{h}$. The convolution with the CIR can be described by multiplication with the corresponding time domain channel matrix $\mathbf{H} \in \mathbb{C}^{(N_{\text{FFT}}+N_{\text{CP}}) \times (N_{\text{FFT}}+N_{\text{CP}})}$. The matrix $\mathbf{H}$ is a lower triangular Toeplitz structured matrix with vector

$$\mathbf{h} = \begin{bmatrix} \text{h}_1 & \text{h}_2 & \dots & \text{h}_{\text{m}} \end{bmatrix}^{\text{T}} \tag{3.6}$$

Die approbierte gedruckte Originalversion dieser Diplomarbeit ist an der TU Wien Bibliothek verfügbar
The approved original version of this thesis is available in print at TU Wien Bibliothek.
TU Bibliothek Your knowledge hub WIEN

at the first column, given by

$$\mathbf{H} = \begin{bmatrix} \mathrm{h}_1 & 0 & \cdots & 0 \\ \mathrm{h}_2 & \mathrm{h}_1 & \ddots & \vdots \\ \vdots & \mathrm{h}_2 & \ddots & 0 \\ \mathrm{h}_\mathrm{m} & \vdots & \ddots & \mathrm{h}_1 \\ 0 & \mathrm{h}_\mathrm{m} & & \mathrm{h}_2 \\ \vdots & 0 & \ddots & \vdots \\ 0 & \cdots & 0 & \mathrm{h}_\mathrm{m} \end{bmatrix}. \tag{3.7}$$

Using the CP whose length exceeds the maximum excess delay of the multipath propagation channel ($N_{\mathrm{CP}} > \mathrm{m}$), a linear convolution is converted into a circular convolution. More precisely, adding and removing the CP turns the Toeplitz structure into a circulant one, given by [18]

$$\mathbf{H}_{\mathrm{cir}} = \mathbf{P}_{\mathsf{remCP}}\mathbf{H}\mathbf{P}_{\mathsf{addCP}} = \begin{bmatrix} \mathrm{h}_1 & \mathrm{h}_\mathrm{m} & \cdots & \mathrm{h}_3 & \mathrm{h}_2 \\ \mathrm{h}_2 & \mathrm{h}_1 & \mathrm{h}_\mathrm{m} & & \mathrm{h}_3 \\ \vdots & \mathrm{h}_2 & \mathrm{h}_1 & \ddots & \vdots \\ \mathrm{h}_{\mathrm{m}-1} & & \ddots & \ddots & \mathrm{h}_\mathrm{m} \\ \mathrm{h}_\mathrm{m} & \mathrm{h}_{\mathrm{m}-1} & \cdots & \mathrm{h}_2 & \mathrm{h}_1 \end{bmatrix}. \tag{3.8}$$

The $\mathbf{H}_{\mathrm{cir}}$ gets diagonalized by the IDFT-DFT operations and the values on the main diagonal are the Fourier transform of the CIR

$$\mathbf{F}_{N_{\mathrm{FFT}}}\mathbf{H}_{\mathrm{cir}}\mathbf{F}^{\mathrm{H}}_{N_{\mathrm{FFT}}} = \mathsf{Diag}(\mathbf{F}_{N_{\mathrm{FFT}}}\mathbf{h}) = \mathbf{H}_{\mathsf{diag}},$$

where operation $\mathsf{Diag}(\cdot)$ places the input vector on the main diagonal of matrix.

The transmitted signal passes the multipath propagation channel and the received signal $\mathbf{r}$ is obtained on the other side. Such a received signal can be compactly formulated by

$$\mathbf{r} = \mathbf{H}\mathbf{s} + \mathbf{n}, \tag{3.9}$$

where $\mathbf{n} \in \mathbb{C}^{(N_{\mathrm{FFT}}+N_{\mathrm{CP}})\times 1}$ represents zero mean i.i.d. white Gaussian noise with $\mathbb{E}\{\mathbf{n}\mathbf{n}^{\mathrm{H}}\} = \sigma_n^2\mathbf{I}_{N_{\mathrm{FFT}}+N_{\mathrm{CP}}}$. After removal of the CP, the received signal is passed through the Discrete Fourier Transform (DFT) block for the transformation to the frequency domain. Received symbol vector $\tilde{\mathbf{y}}$ is hence given by

$$\tilde{\mathbf{y}} = \mathbf{F}_{N_{\mathrm{FFT}}}\mathbf{P}_{\mathsf{remCP}}\mathbf{r} = \mathbf{F}_{N_{\mathrm{FFT}}}\mathbf{P}_{\mathsf{remCP}}\mathbf{H}\mathbf{P}_{\mathsf{addCP}}\mathbf{F}^{\mathrm{H}}_{N_{\mathrm{FFT}}}\tilde{\mathbf{x}} + \mathbf{w} = \mathbf{H}_{\mathsf{diag}}\tilde{\mathbf{x}} + \mathbf{w}, \tag{3.10}$$

where $\mathbf{F}_{N_{\mathrm{FFT}}}$ is the standard $N_{\mathrm{FFT}} \times N_{\mathrm{FFT}}$ DFT matrix,

$$\mathbf{P}_{\mathsf{remCP}} = [\,\mathbf{0} \;\; \mathbf{I}_{N_{\mathrm{FFT}}}] \tag{3.11}$$

Die approbierte gedruckte Originalversion dieser Diplomarbeit ist an der TU Wien Bibliothek verfügbar
The approved original version of this thesis is available in print at TU Wien Bibliothek.
TU Bibliothek Your knowledge hub WIEN

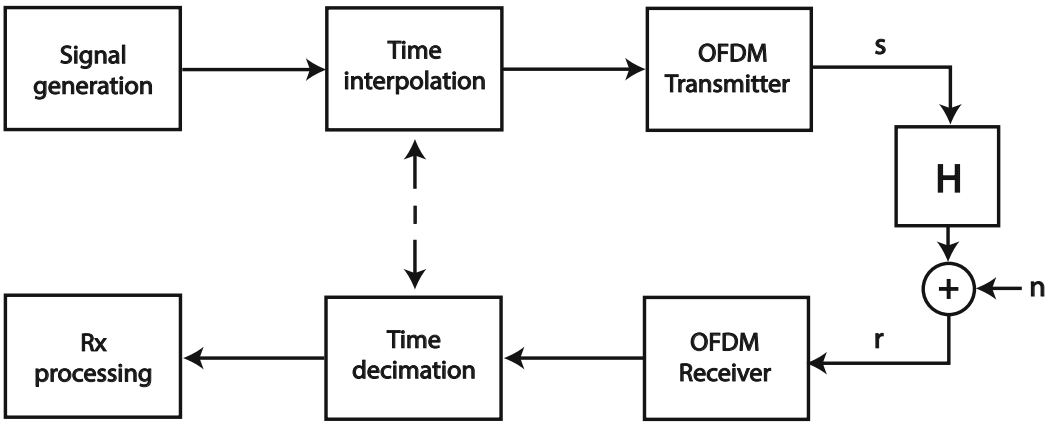

Figure 3.2: By enlarging the symbol length T^I by an interpolation factor I, it is possible to emulate a velocity v^I while conducting measurements at an actual speed v.

describes the removal of the CP of length N_{CP} and

$$\mathbf{w} = \mathbf{F}_{N_{\mathrm{FFT}}} \mathbf{P}_{\mathrm{remCP}} \mathbf{n}. \tag{3.12}$$

To remove effects induced by the multipath propagation channel, a zero-forcing (ZF) equalizer $\mathbf{D}$ of size $\mathbf{D} \in \mathbb{C}^{N_{\mathrm{FFT}} \times N_{\mathrm{FFT}}}$ is employed. Thus, the data estimates $\tilde{\mathbf{x}}_{\mathrm{est}}$ of the received signal $\mathbf{r}$ are given by

$$\tilde{\mathbf{x}}_{\mathrm{est}} = \mathbf{D}\tilde{\mathbf{y}} = \mathbf{D}(\mathbf{H}_{\mathrm{diag}}\tilde{\mathbf{x}} + \mathbf{w}). \tag{3.13}$$

Such an equalizer structure can be computationally rather complex. Fortunately, due to the employed CP in the OFDM processing, the equalizer takes on a diagonal structure. Furthermore, to discard $(N_{\mathrm{FFT}} - N)$ zeros appended at the transmitter, the $N \times N_{\mathrm{FFT}}$ matrix $\mathbf{R}_{N_{\mathrm{FFT}}}$ is employed. Thus, the data estimates are given by

$$\mathbf{x}_{\mathrm{est}} = \mathbf{R}_{N_{\mathrm{FFT}}} \tilde{\mathbf{x}}_{\mathrm{est}}, \tag{3.14}$$

where

$$\mathbf{R}_{N_{\mathrm{FFT}}} = [\, \mathbf{I}_N \;\; \mathbf{0}]. \tag{3.15}$$

So far, I described a multipath propagation channel without considering its changes over time. If the multipath channel is time-invariant, the channel matrix $\mathbf{H}_{\mathrm{diag}}$ remains a diagonal matrix. In that case, the received signal is free of Inter-Carrier-Interference (ICI). On the other side, if the multipath channel is time-variant, the channel matrix $\mathbf{H}_{\mathrm{diag}}$ is not diagonal. More precisely, non-zero elements will appear outside the main diagonal of $\mathbf{H}$ and ICI arises in the received signal.

Die approbierte gedruckte Originalversion dieser Diplomarbeit ist an der TU Wien Bibliothek verfügbar
The approved original version of this thesis is available in print at TU Wien Bibliothek.
TU Bibliothek Your knowledge hub WIEN

The amount of ICI is related with the normalized Doppler spread D_{n} of the channel. The normalized Doppler spread is given by

$$D_{\mathrm{n}} = f_{D_{\max}} \cdot T, \tag{3.16}$$

where $f_{D_{\max}}$ and $T = T_{\mathrm{s}} \cdot N$ represent the maximum Doppler frequency and the symbol duration, respectively. As proposed in [11], parameter T can be adjusted by time interpolation by a factor I, yielding a symbol duration

$$T^I = I \cdot T_{\mathrm{s}} \cdot N. \tag{3.17}$$

Consequently, an interpolation by a factor I corresponds to a reduction of the subcarrier spacing

$$\triangle f = \frac{1}{T_{\mathrm{s}}} = \frac{f_{\mathrm{s}}}{N_{\mathrm{FFT}}}, \tag{3.18}$$

by the same factor I, given by

$$\triangle f^I = \frac{1}{I \cdot T_{\mathrm{s}}} = \frac{1}{I}\frac{f_{\mathrm{s}}}{N_{\mathrm{FFT}}}, \tag{3.19}$$

where f_{s} and N_{FFT} represent sampling rate and FFT length, respectively. By taking the proposed time interpolation into account, the normalized Doppler spread can be rewritten as:

$$D_{\mathrm{n}}^I = f_{D_{\max}} \cdot T^I = f_{D_{\max}} \cdot I \cdot T_{\mathrm{s}} \cdot N = \frac{T_{\mathrm{s}} \cdot N \cdot I \cdot f_{\mathrm{c}} \cdot v}{c} = \frac{T_{\mathrm{s}} \cdot N \cdot f_{\mathrm{c}}}{c} \cdot v^I \tag{3.20}$$

where f_{c}, c, $v^I = I \cdot v$ and I represent the carrier frequency of a signal, the speed of light, the emulated speed as a result of an actual measurement speed v and an interpolation factor, respectively. As shown in (3.20), by enlarging the symbol length T^I by an interpolation factor I, it is possible to emulate a velocity v^I while conducting measurements at an actual speed v. In addition, the described method can also be used to emulate speeds lower than the actual one by taking $0 < I < 1$. Finally, note also that I does not have to be an integer value, hence providing great flexibility for adjusting v^I from v [11]. The block diagram of an OFDM transceiver which employs above described interpolation method is shown in Figure 3.2.

There are several methods to perform the time interpolation proposed in [14]. One group of methods is based on signal resampling, while the other is based on the insertion of additional subcarriers between original data subcarriers.

Die approbierte gedruckte Originalversion dieser Diplomarbeit ist an der TU Wien Bibliothek verfügbar
The approved original version of this thesis is available in print at TU Wien Bibliothek.
TU Bibliothek Your knowledge hub WIEN

3.2 Resample & Repeat

One possible method to perform time-stretching is to change the sampling rate f_{s} of given multi-carrier signal by a factor of I, provided by

$$f_{\mathrm{s}}^{I} = \frac{f_{\mathrm{s}}}{I}. \tag{3.21}$$

The changing of sampling rate or resampling needs to be done at both the transmitter and the receiver, while FFT size N_{FFT} remains unchanged. Thereby, subcarrier spacing $\triangle f^{I}$ is decreased by a factor of I compared to the subcarrrier spacing of original signal $\triangle f$, which can be written as

$$\triangle f^{I} = \frac{f_{\mathrm{s}}^{I}}{N_{\mathrm{FFT}}} = \frac{1}{I}\frac{f_{\mathrm{s}}}{N_{FFT}} = \frac{\triangle f}{I}. \tag{3.22}$$

Decrease in the subcarrier spacing $\triangle f$ by a factor of I decreases the signal bandwidth B by the same factor. More precisely, the bandwidth of resampled signal B^{I} is I times smaller than the bandwidth of original signal B, which is then given by

$$B^{I} = N \cdot \triangle f^{I} = N\frac{\triangle f}{I} = \frac{B}{I}. \tag{3.23}$$

In order to compare the resampled signal with the original one in a fair manner, they need to occupy the same total bandwidth B. Therefore, the resampled signal with the bandwidth $\frac{B}{I}$ is repeated I times in the frequency domain. Hence, such resampled and repeated signal occupies the same total bandwidth as the original signal. Such a transformation is shown in Figure 3.3 and the modified OFDM signal in the frequency domain can be represented as vector $\mathbf{x}^{R\&R} \in \mathbb{C}^{NI\times 1}$, given by

$$\begin{aligned} \mathbf{x}^{R\&R} &= \begin{bmatrix}\mathbf{x}^{(1)} & \mathbf{x}^{(2)} & \dots & \mathbf{x}^{(I)}\end{bmatrix}^{\mathsf{T}} \\ &= \begin{bmatrix}\mathrm{x}_1^{(1)} & \mathrm{x}_2^{(1)} & \dots & \mathrm{x}_N^{(1)} & \dots & \mathrm{x}_1^{(I)} & \mathrm{x}_2^{(I)} & \dots & \mathrm{x}_N^{(I)}\end{bmatrix}^{\mathsf{T}}, \end{aligned} \tag{3.24}$$

where $\mathbf{x}^{(i)}$ represent i-th replica $(i = 1, \dots, I)$ of frequency-domain OFDM signal $\mathbf{x}$. According to procedure explained in Section 5.2, the $\mathbf{x}^{R\&R}$ is then processed by the OFDM modulator with the sampling rate f_{s}^{I}. Thereafter, the transmit signal is passed over time-variant multipath propagation channel, while receiver moves at an actual speed v.

On the receiver side, the signal is processed by the OFDM demodulator with the sampling rate f_{s}^{I} and equalized, according to procedure explained in Section 5.2. Thus, the estimate $\mathbf{x}_{\mathrm{est}}^{R\&R}$ of the received signal is obtained, which can be represented as

$$\mathbf{x}_{\mathrm{est}}^{R\&R} = \begin{bmatrix}\mathbf{x}_{\mathrm{est}}^{(1)} & \mathbf{x}_{\mathrm{est}}^{(2)} & \dots & \mathbf{x}_{\mathrm{est}}^{(I)}\end{bmatrix}^{\mathsf{T}}. \tag{3.25}$$

Die approbierte gedruckte Originalversion dieser Diplomarbeit ist an der TU Wien Bibliothek verfügbar
The approved original version of this thesis is available in print at TU Wien Bibliothek.
TU Bibliothek Your knowledge hub WIEN

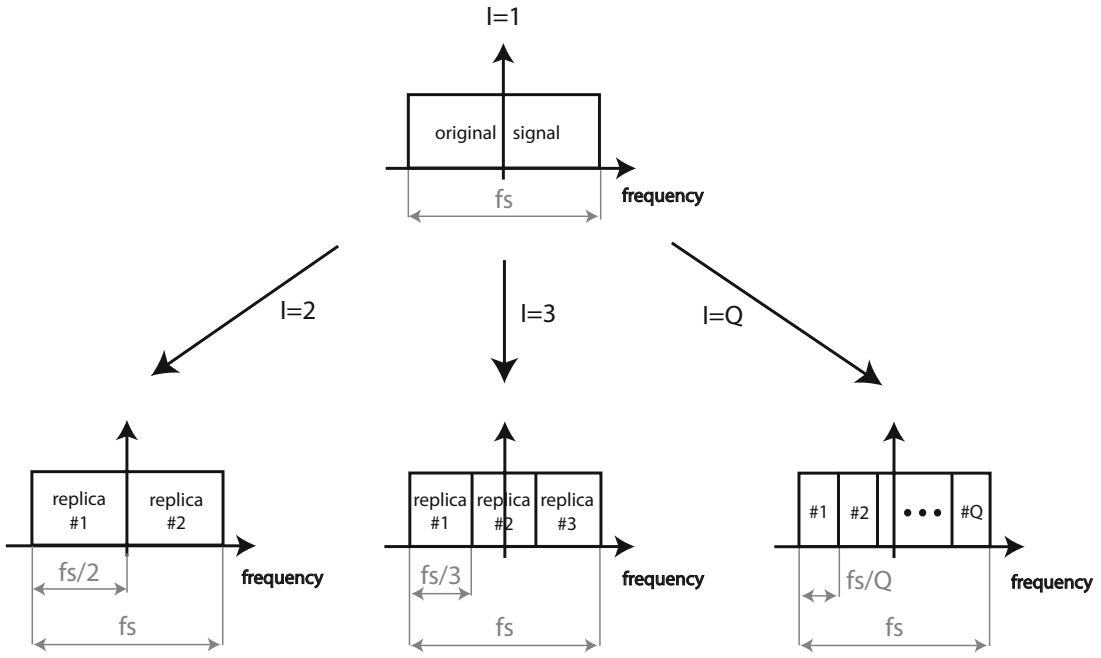

Figure 3.3: Resample & Repeat method: The original signal is the resampled and thereafter repeated I times in the frequency domain to occupy the same bandwidth as the original signal.

The $\mathbf{x}_{\text{est}}^{R\&R}$ consists of I estimated replicas which can be then averaged, which can be represented as

$$\mathbf{x}_{\text{est}} = \frac{1}{I}\sum_{i=1}^{I}\mathbf{x}_{\text{est}}^{(i)}. \tag{3.26}$$

3.3 Random Symbols

Another method to perform time-stretching by changing the subcarrier spacing $\triangle f$ is to increase the FFT length N_{FFT} by an integer factor $I > 1$

$$N_{\text{FFT}}^{I} = N_{\text{FFT}} \cdot I, \tag{3.27}$$

while sampling rate f_{s} remains unchanged. This is done by inserting $(I-1)$ additional subcarriers between the original ones at the transmitter. The role of additional subcarriers is to mimic the ICI, as receiver is moving at velocity v^I while conducting measurements at an actual speed v. Therefore, such additional subcarriers should not be equal to zero. The insertion of additional subcarriers is shown in Figure 3.4 and corresponding OFDM signal in frequency domain can be represented as vector

Die approbierte gedruckte Originalversion dieser Diplomarbeit ist an der TU Wien Bibliothek verfügbar
The approved original version of this thesis is available in print at TU Wien Bibliothek.

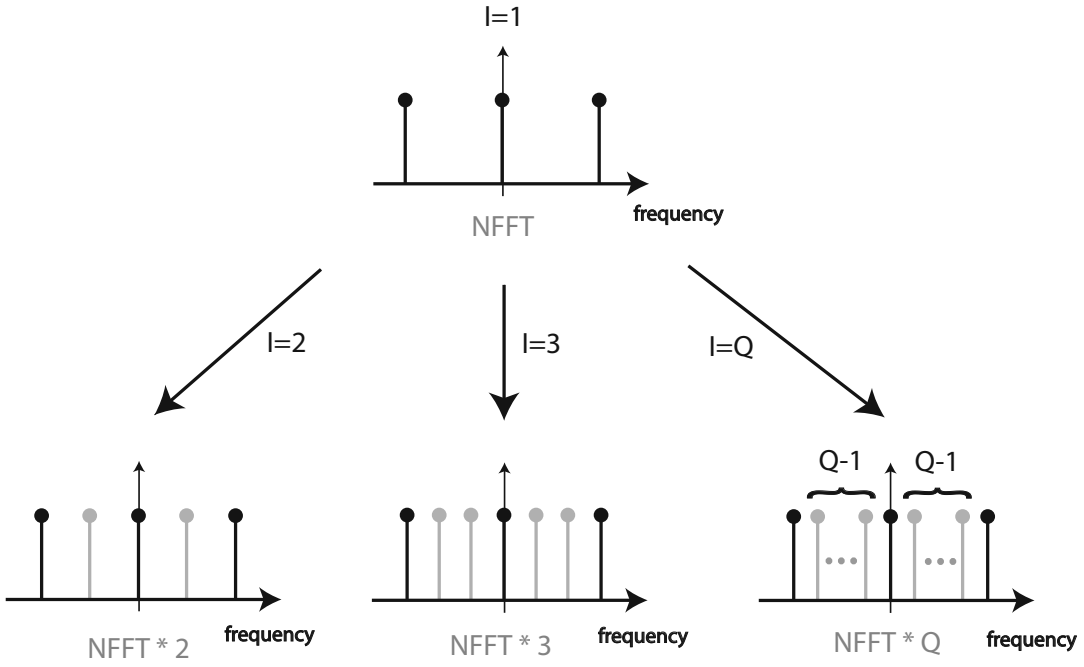

Figure 3.4: Random Symbols method: Additional random subcarriers are inserted between the original data subcarriers to mimic the ICI, as receiver is moving at velocity v^I, while conducting measurements at an actual speed v.

$\mathbf{x}^{RS} \in \mathbb{C}^{[N+(N-1)(I-1)]\times 1}$, given by

$$\mathbf{x}^{RS} = \mathbf{x}^I + \mathbf{c}, \tag{3.28}$$

where $\mathbf{x}^I \in \mathbb{C}^{[N+(N-1)(I-1)]\times 1}$ and $\mathbf{c} \in \mathbb{C}^{[N+(N-1)(I-1)]\times 1}$ represent data and random subcarriers, respectively. The $\mathbf{x}^I$ is given by

$$\mathbf{x}^I = \begin{bmatrix} \mathrm{x}_1 & \mathbf{0}_{(I-1)} & \mathrm{x}_2 & \dots & \mathrm{x}_{N-1} & \mathbf{0}_{(I-1)} & \mathrm{x}_{N-1} \end{bmatrix}^{\mathsf{T}} \tag{3.29}$$

with $(I-1)$ zeros $\mathbf{0}_{(I-1)}$ between each data subcarrier, while $\mathbf{c}$ is given by

$$\mathbf{c} = \begin{bmatrix} 0 & \mathbf{c}_1 & 0 & \dots & 0 & \mathbf{c}_{N-1} & 0 \end{bmatrix}^{\mathsf{T}} \tag{3.30}$$

with $(I-1)$ additional subcarriers denoted by vector $\mathbf{c}_i$ $(i = 1, \dots, N-1)$ inserted between each subcarrier. As can be observed, the $\mathbf{x}^I$ and the $\mathbf{c}$ are restricted to lie in disjoint frequency subspaces. Inserted subcarriers are chosen to be random, thereby decreasing the PAPR compared to "Resample & Repeat" method [14]. According to procedure explained in Section 5.2, the $\mathbf{x}^{RS}$ is then processed by the OFDM modulator with the FFT size N^I_{FFT} and passed over time-variant multipath propagation channel,

Die approbierte gedruckte Originalversion dieser Diplomarbeit ist an der TU Wien Bibliothek verfügbar
The approved original version of this thesis is available in print at TU Wien Bibliothek.
TU Bibliothek Your knowledge hub WIEN

while receiver moves at an actual speed v.

On the receiver side, the signal is processed by the corresponding OFDM demodulator and equalized. As the result, the estimate $\mathbf{x}_{\text{est}}^{RS}$ of the received signal is obtained, which can be represented as

$$\mathbf{x}_{\text{est}}^{RS} = \mathbf{x}_{\text{est}}^{I} + \mathbf{c}_{\text{est}} \tag{3.31}$$

Since additional subcarriers were introduced only to mimic the ICI in the time-variant propagation channel, they need to be discarded. Hence, only the estimates of data subcarriers are extracted, which can be described as

$$\mathbf{x}_{\text{est}} = \begin{bmatrix} \mathrm{x}_{\text{est},1}^{RS} & \mathrm{x}_{\text{est},2I-I+1}^{RS} & \cdots & \mathrm{x}_{\text{est},NI-I+1}^{RS} \end{bmatrix}^{\mathsf{T}}. \tag{3.32}$$

By keeping the sampling frequency the same as for the original signal ($f_{\text{s}}^{I} = f_{\text{s}}$), the symbol length is thereby increased by the factor I and the subcarrier spacing is decreased by the same factor. Such method can be written as

$$\triangle f^{I} = \frac{f_{\text{s}}}{N_{\text{FFT}}^{I}} = \frac{1}{I}\frac{f_{\text{s}}}{N_{\text{FFT}}} = \frac{\triangle f}{I}. \tag{3.33}$$

Compared to the "Resample & Repeat" time-stretching method, this method preserves the bandwidth of the original signal ($B^{I} = B$) by keeping the initial sampling frequency and inserting additional subcarriers.

Die approbierte gedruckte Originalversion dieser Diplomarbeit ist an der TU Wien Bibliothek verfügbar
The approved original version of this thesis is available in print at TU Wien Bibliothek.
TU Bibliothek Your knowledge hub WIEN

Die approbierte gedruckte Originalversion dieser Diplomarbeit ist an der TU Wien Bibliothek verfügbar
The approved original version of this thesis is available in print at TU Wien Bibliothek.

4 Channel estimation

In this section, I consider an auxiliary unwanted channel estimation side effect of the "Resample & Repeat" interpolation method. To overcome this effect, I adapt the pilot-based channel estimation scheme within the "Resample & Repeat" interpolation method. The adapted channel estimation scheme is described in Section 4.2. The simulation-based comparison in terms of channel estimation Minimum Square Error (MSE) is provided in Section 4.3.

4.1 Motivation

To mitigate distortions introduced by the wireless channel, the Channel State Information (CSI) is required. In mobile communications, the CSI is usually not known at the receiver. Therefore, it needs to be estimated. One simple and popular channel estimation method in multi-carrier systems is pilot-aided channel estimation. Pilot symbols, which are well-known at the receiver, are inserted between data symbols in both the time and frequency domain. These pilot symbols enable the estimation of channel coefficients at pilot positions. Thereafter, channel coefficients at data positions are estimated through interpolation. The interpolation can be performed in frequency-domain, time-domain or in both frequency- and time-domain.

As already explained in Sections 3.2 and 3.3, proposed interpolation methods stretch the signal in time to emulate higher receiver velocities by conducting measurements at lower velocities. Thus, the time duration of a time-stretched signal corresponds to the duration of the original signal at the velocity to be emulated. This is also valid for the time-domain pilot spacing and therefore for resulting time-domain channel interpolation errors. In the frequency-domain, on the other hand, differences arise due to a changed arrangement of symbols.

In the case of the "Random Symbols" interpolation method, the insertion of additional subcarriers decreases the sampling rate, but it does not change the frequency distance between the original subcarriers. Therefore, the original frequency-domain pilot spacing is preserved in the case of the "Random Symbols" interpolation method. Consequently, there is no improvement or decrease of channel estimation with increasing the factor I in a frequency-selective channel. Such pilot-insertion scheme is illustrated in Figure 4.1b.

On the other hand, in the case of the "Resample & Repeat" interpolation method, the pilot spacing in the frequency-domain decreases with an interpolation factor I. Apart from the decrease of the pilot spacing, the number of pilot symbols is increased by the factor I when repeating the original signal I times. Such unwanted spectral

Die approbierte gedruckte Originalversion dieser Diplomarbeit ist an der TU Wien Bibliothek verfügbar
The approved original version of this thesis is available in print at TU Wien Bibliothek.
TU Bibliothek Your knowledge hub WIEN

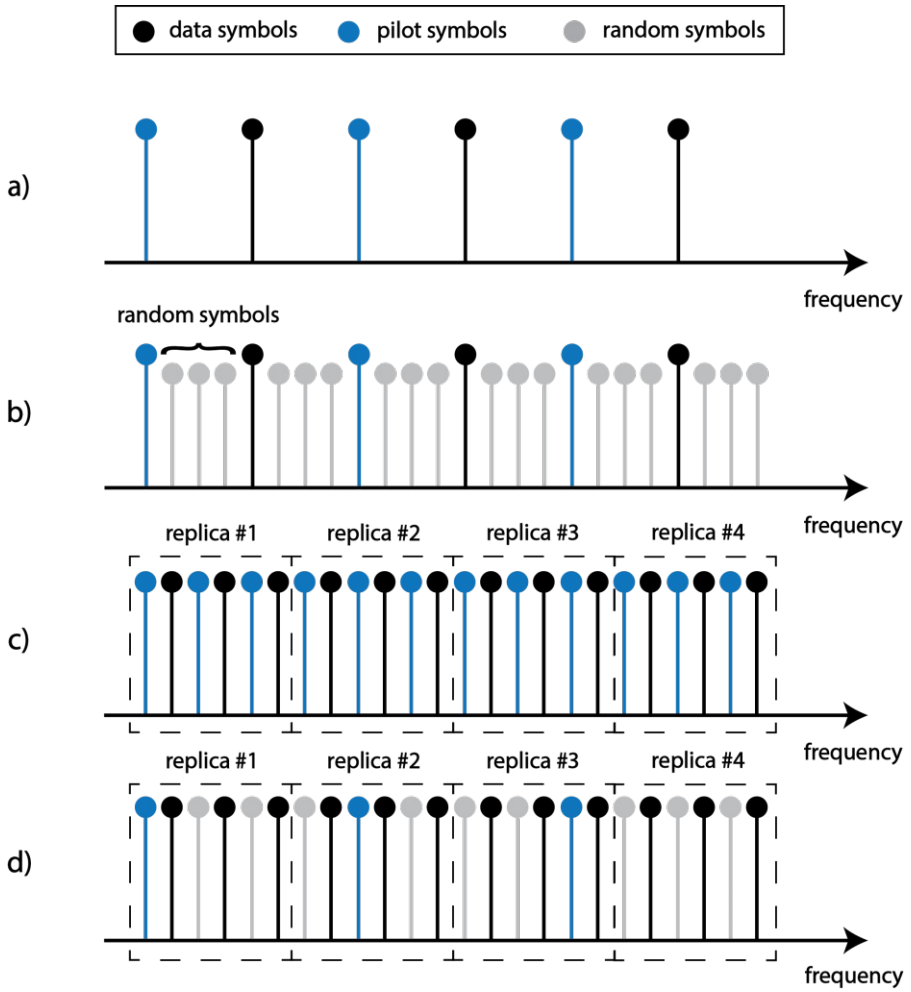

Figure 4.1: Pilot insertion schemes for I=4: a) original signal, b) random symbols, c) resample & repeat - decreased spacing, d) resample & repeat - equal spacing

side effect (shown in Figure 4.1c) leads to an improvement of the channel estimation in a multipath propagation channel with increasing the factor I. Consequently, the "Resample & Repeat" and the "Random Symbols" interpolation methods cannot be compared in a fair manner in practical systems, due to the different quality of channel estimation. Unfortunately, due to such channel estimation side effect, the comparison can only be performed in a simulation environment, where the full CSI is known to the receiver.

Die approbierte gedruckte Originalversion dieser Diplomarbeit ist an der TU Wien Bibliothek verfügbar
The approved original version of this thesis is available in print at TU Wien Bibliothek.
TU Bibliothek Your knowledge hub WIEN

4.2 Adapted channel estimation scheme

To compare the "Resample & Repeat" and the "Random Symbols" interpolation methods in a fair manner, I adapt pilot-based channel estimation scheme within the "Resample & Repeat" interpolation method. The principle is as follows. Instead of the pilot insertion before resampling and repeating in the frequency domain, this scheme inserts pilot symbols after the signal is resampled and repeated. Furthermore, the spacing between pilot symbols of the interpolated system in the frequency domain is increased by the factor I. Therefore, the frequency-domain pilot spacing is preserved and corresponds to the pilot spacing of the original signal. The proposed scheme is illustrated in Figure 4.1d, where a difference between the previously used (Figure 4.1c) and proposed pilot scheme (Figure 4.1d) can be noticed.

Besides the main purpose explained above, the adapted channel estimation scheme poses an additional one. Since the proposed scheme is based on skipping the pilot symbols used in the initial scheme (Figure 4.1c), these symbols remain unused. Thus, the adapted scheme opens up the possibility of using skipped symbols for other purposes. The main role of skipped symbols is to mimic the ICI, as the receiver is

Table 4.1: Simulation Parameters for Channel Estimation

Parameter	Value
Carrier Frequency	2.5 GHz
Symbol Alphabet	64-QAM
Number of Subcarriers	24
Symbols per Frame	14
Number of Realizations	1000
Sampling Rate	15.36 MHz
FFT Size	1024
Bandwidth	360 kHz
Interpolation Factor	1, 2, 4, 8
Receiver Velocity	0 km/h
SNR	100 dB
Channel Power Delay Profile	PedestrianB
Channel Doppler Model	Jakes
Pilot Pattern	Rectangular
Frequency-domain Pilot Spacing	4
Time-domain Pilot Spacing	1
Interpolation Method	Linear

Die approbierte gedruckte Originalversion dieser Diplomarbeit ist an der TU Wien Bibliothek verfügbar
The approved original version of this thesis is available in print at TU Wien Bibliothek.
TU Bibliothek Your knowledge hub WIEN

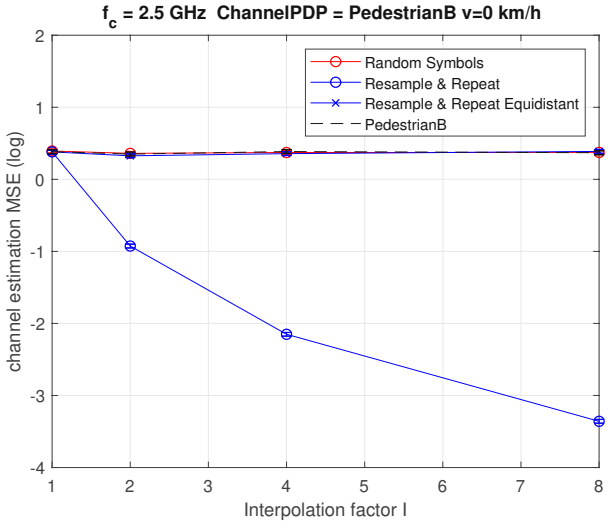

Figure 4.2: By using adapted pilot-based channel estimation scheme, the original frequency-domain pilot spacing is preserved and the "Resample & Repeat" and the "Random Symbols" interpolation methods can be compared in a fair manner.

moving at velocity v^I while conducting measurements at an actual speed v. Therefore, such skipped symbols should not be equal to zero.

4.3 Simulation-based comparison

For the evaluation of adapted pilot-based channel estimation scheme, I performed simulation-based comparison in terms of the channel MSE using the Vienna 5G Link Level Simulator [19, 20]. The simulation parameters are given in Table 4.1. Firstly, I evaluated the mean squared channel estimation and interpolation error

$$\mathrm{MSE} = \frac{1}{R}\frac{1}{K}\frac{1}{N}\sum_{r=1}^{R}\sum_{k=1}^{K}\sum_{n=1}^{N}|\hat{\mathrm{H}}_{k,n,r} - \mathrm{H}_{k,n,r}|^2. \tag{4.1}$$

In (4.1), $\hat{\mathrm{H}}_{k,n,r}$ denotes the estimated channel coefficient and $\mathrm{H}_{k,n,r}$ is the actual channel coefficient at subcarrier n, time symbol k and channel realization r. The simulation results are shown in Figure 4.2a. As a comparison reference, I used MSE for PedestrianB delay profile, when no interpolation method is employed. In other words, the channel is generated for each actual velocity of the receiver. For the "Random Symbols" interpolation method, the original pilot spacing is preserved and consequently, there is no difference in channel estimation quality when compared with the PedestrianB reference without interpolation methods employed. In the case of "Resample & Repeat"

Die approbierte gedruckte Originalversion dieser Diplomarbeit ist an der TU Wien Bibliothek verfügbar
The approved original version of this thesis is available in print at TU Wien Bibliothek.
TU Bibliothek Your knowledge hub WIEN

interpolation method, when pilot-scheme with decreased pilot spacing is employed, one can observe that MSE decreases with the number I of repetitions. In other words, the channel estimation quality improves with the number I of repetitions. As explained before, it occurs due to the larger number and more dense distribution of pilot symbols in the frequency domain. On the other hand, when using the adapted pilot-based channel estimation scheme with equidistant pilot spacing, one can observe constant MSE performance over the number of repetitions, which was the goal of this method.

Die approbierte gedruckte Originalversion dieser Diplomarbeit ist an der TU Wien Bibliothek verfügbar
The approved original version of this thesis is available in print at TU Wien Bibliothek.
TU Bibliothek Your knowledge hub WIEN

Die approbierte gedruckte Originalversion dieser Diplomarbeit ist an der TU Wien Bibliothek verfügbar
The approved original version of this thesis is available in print at TU Wien Bibliothek.

5 PAPR reduction methods

This section considers the issue of increased Peak-to-Average power ratio (PAPR) when using "Resample & Repeat" and "Random Symbols" interpolation methods. The causes of increased PAPR are explained in Section 5.1. Thereafter, in Section 5.2, I give a brief introduction to existing PAPR reduction techniques. In order to overcome the problem of increased PAPR, I adapt existing PAPR reduction techniques, such that interpolation methods can be used in practical communication systems more efficiently. This chapter includes the following novel contributions:

- In Section 5.3, I adapt frequency-domain techniques, such as Interleaving and Selective Mapping on random symbols to reduce the PAPR.
- In order to overcome the high complexity of frequency-domain PAPR reduction techniques, I propose adapted time-domain techniques in Section 5.4.

In Section 5.5, I provide a comparative overview of PAPR reduction methods in terms of reduction capability, computational complexity and power increase. This overview allows for an easier choice of PAPR reduction technique for a specific application.

5.1 Motivation

Proposed interpolation methods are intended for use in HST real-world experiments where one has to cope with hardware limitations and impairments. One of the most challenging unresolved issues in the hardware implementation of multi-carrier systems is the resulting non-constant envelope with high peaks [21]. Basically, a multi-carrier system consists of a large number of independently modulated subcarriers. If these subcarriers are added coherently, the instantaneous power will be larger than the average power.

Consider the OFDM signal in time domain $\mathbf{s}$ described in Section 5.2, where N subcarriers are added together. If N is large enough, then, based on central-limit theorem (CLT), the resulting signal $\mathbf{s}$ in the time domain will be close to a complex Gaussian process [22]. This means that both of its real and imaginary parts are Gaussian distributed and its envelope and power follows Rayleigh and exponential distributions, respectively. If the instantaneous amplitudes of the different subcarriers have high peaks aligned at the same time, the envelope of resulting signal $\mathbf{s}$ will exhibit high peaks. The Peak-to-Average power ratio (PAPR) is the ratio between the maximum and the average power of a sample in a given transmit symbol $\mathbf{s}$ and is usually expressed in the units of dB,

$$\mathrm{PAPR}\,[\mathrm{dB}] = 10 \log \left(\frac{\max\left\{|\mathbf{s}|^2\right\}}{\mathrm{E}\left\{|\mathbf{s}|^2\right\}} \right), \tag{5.1}$$

Die approbierte gedruckte Originalversion dieser Diplomarbeit ist an der TU Wien Bibliothek verfügbar
The approved original version of this thesis is available in print at TU Wien Bibliothek.
TU Bibliothek Your knowledge hub WIEN

where $\mathrm{E}\{\cdot\}$ is the expectation operator. For the OFDM system with M-QAM modulation format, which is considered in this section, the signal constellation has varying signal power levels over different constellation points. According to the conclusion of [23], the upper bound of the PAPR in OFDM-QAM systems can be derived out

$$\frac{3N}{M-1} \leq \mathrm{PAPR}_{\max} \leq \frac{3N\left(\sqrt{M}-1\right)^2}{M-1}, \tag{5.2}$$

where M represents the QAM modulation order. From (5.2), one can observe that the PAPR depends on the modulation order M and number of subcarriers N.

Increased PAPR impacts the design of a transmission system or, more precisely, the selection of a power amplifier at the transmitter. Suppose the transmitter uses a high-efficiency non-linear power amplifier that operates near the saturated region. In that case, although the mean signal amplitude lies within the power amplifier's linear operating region, signal peaks of large amplitude fall into the saturated region. In this region, the output signal is being compressed and increasing the input power does not produce a corresponding increase in the output power. Apart from the signal compression, spectral regrowth and OOB radiation of the multi-carrier signal can occur. To avoid these phenomena, the power amplifier needs to operate in the linear region, which reduces the efficiency. However, the PAPR issue is not critical in the downlink case, where an expensive power amplifier can be used at the transmitter. In the uplink case, the PAPR issue is critical, since the transmitter is a small mass-market mobile device. Apart from degrading the efficiency of a power amplifier for a given average transmit power, the ICI caused by nonlinearities in the transmission chain increases with the PAPR [14]. Therefore, high PAPR is one of the major drawbacks of a multi-carrier transmission system.

Compared to the conventional multi-carrier systems, the PAPR issue becomes even worse if interpolation methods are employed on multi-carrier signals. Both interpolation methods described in Section 3 are based on an increase of a number of subcarriers N with an interpolation factor I. According to (5.2), an increase in N results in an increase in the maximum PAPR. In addition, if the "Resample & Repeat" interpolation method is employed, the same signal is repeated I times in the frequency domain. Since the instantaneous amplitudes of the repeated signal replicas have high peaks aligned simultaneously, the resulting signal will exhibit a substantial increase of the PAPR with the interpolation factor I. On the other hand, the "Random Symbols" interpolation method is based on the insertion of random subcarriers between data subcarriers. Since this method does not repeat the same signal, the increase in the PAPR is not significant, compared to the case of the "Resample & Repeat" interpolation method.

Die approbierte gedruckte Originalversion dieser Diplomarbeit ist an der TU Wien Bibliothek verfügbar
The approved original version of this thesis is available in print at TU Wien Bibliothek.
TU Bibliothek Your knowledge hub WIEN

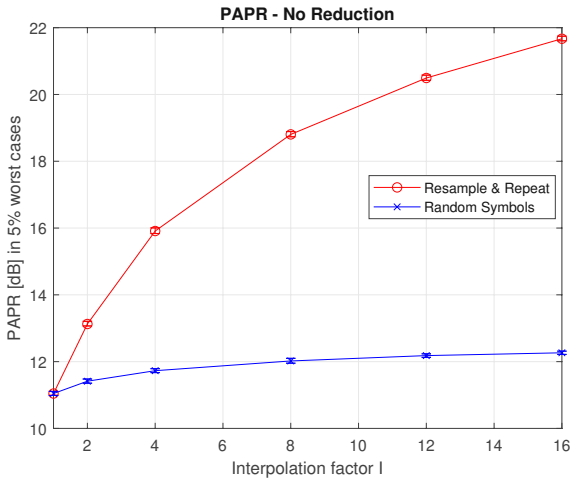

Figure 5.1: Due to multiple repetitions of the same signal, "Resample & Repeat interpolation method exhibits significant increase of the PAPR with the interpolation factor I.

To emulate high speeds by performing measurements at low speeds, it is necessary to use a higher interpolation factor I. The use of higher interpolation factors I results in a PAPR increase for both "Resample & Repeat" and "Random Symbols" interpolation methods. This effect can be observed in Figure 5.1, where the PAPR values in 5% worst cases are calculated over different interpolation factors. More precisely, for each interpolation factor and for N_r realizations, I calculate the PAPR according to (5.1). Thereafter, I take 5% worst PAPR values of N_r realizations and calculate their average PAPR value for each interpolation factor (used parameters given in Table 5.1). Therefore, to use a higher interpolation factor I in practical systems without degrading the efficiency of a power amplifier, it is necessary to reduce the PAPR for both interpolation methods.

5.2 Introduction to PAPR reduction methods

There are many proposed classical techniques to reduce the PAPR. These techniques include amplitude clipping and filtering [24, 25, 26, 27], tone reservation [28, 29], partial transmit sequence (PTS) [30, 31, 32, 33, 34, 35], selective mapping [36, 37, 38, 39, 40] and interleaving [41, 42, 43, 44]. Although there are many techniques for PAPR reduction, most of them transform the transmit signal to reduce the PAPR. Therefore, besides the data signal, such techniques require to transmit side information bits, in order to inform the receiver how to transform back the received signal. Such a transmit side information introduces an overhead in a transmission

Die approbierte gedruckte Originalversion dieser Diplomarbeit ist an der TU Wien Bibliothek verfügbar
The approved original version of this thesis is available in print at TU Wien Bibliothek.
TU Bibliothek Your knowledge hub WIEN

system.

To avoid the introduced transmission overhead, I adapt above mentioned PAPR reduction techniques. As described in Section 3.3, the "Random Symbols" interpolation method is based on the insertion of $(I-1)$ random symbols between each data symbol. My adapted techniques are based on a transformation of random symbols only, while data symbols remain unchanged. On the other hand, the "Resample & Repeat" interpolation method (described in Section 3.2) resamples and repeats the same signal consisting of data symbols only, whereby no random symbols are employed. Fortunately, the modified pilot-based channel estimation scheme proposed in Section 4.2 provides a possibility of utilizing random symbols in the "Resample & Repeat" interpolation method. More precisely, this pilot scheme inserts pilot symbols after the signal is resampled and repeated with a pilot spacing I times larger than the nominal pilot spacing P. Such pilot spacing leaves skipped symbols (previously used as pilot symbols) unused. I consider these unused symbols to be random and furthermore transform them in order to reduce the PAPR. Such usage of skipped symbols represents another advantage of the proposed pilot scheme, in addition to the channel estimation.

Hence, both "Random Symbols" and "Resample & Repeat" interpolation methods have a possibility to transform random symbols only to reduce the PAPR. Since the role of random symbols is to mimic the ICI and data symbols remain unchanged, there is no impact of PAPR reduction techniques on interpolation methods. Apart from this, since random symbols are neglected at the receiver, there is no need to transmit side information bits to transform back such symbols in their original form. Thus, employing the PAPR reduction techniques to random symbols only, there is no overhead introduced in a transmission system. However, since the proposed interpolation methods significantly differ from each other, the goal is to find an effective PAPR reduction technique that suits the best for a specific interpolation method. In addition, it is necessary to find a method that gives the best trade-off between the extent of PAPR reduction and computational complexity.

In this section, I compare adapted PAPR reduction techniques by means of simulations. Thereby, I use simulation parameters given in Table 5.1. I divided PAPR reduction methods into frequency-domain and time-domain reduction methods, depending on whether the reduction or more precisely, random symbol transformation was performed prior to the IDFT or after the IDFT.

5.3 Frequency-domain reduction methods

Frequency-domain reduction methods perform a transformation of random symbols prior to the IDFT. More precisely, random symbols are transformed, combined with

Die approbierte gedruckte Originalversion dieser Diplomarbeit ist an der TU Wien Bibliothek verfügbar
The approved original version of this thesis is available in print at TU Wien Bibliothek.
TU Bibliothek Your knowledge hub WIEN

Table 5.1: Simulation Parameters for PAPR Calculation

Parameter	Value
Symbol Alphabet	64-QAM
Number of Subcarriers	24
Symbols per Frame	14
Carrier Frequency	2.5 GHz
Sampling Rate	15.36 MHz
FFT Size	1024
Bandwidth	360 kHz
Interpolation Factor	1, 2, 4, 8, 12, 16
Number of Iterations	100
Number of Realizations	3000

data symbols and the IDFT is then performed to obtain a time-domain signal. On such a time-domain signal, the PAPR is calculated. Then, the whole procedure is repeated until the minimum PAPR is found.

Let us assume that data symbols and random symbols (interpolation method not specified) are denoted with $\mathbf{x}^I$ and $\mathbf{c}$, respectively, where $\mathbf{c}$ is defined as

$$\mathbf{c} = [\mathrm{c}_1 \ \mathrm{c}_2 \ \ldots \ \mathrm{c}_L]^{\mathrm{T}} \tag{5.3}$$

and L denotes the length of random symbol vector $\mathbf{c}$. In the case of the "Resample & Repeat" interpolation method the length of random symbol vector is given by

$$L^{R\&R} = \left[\frac{N}{P} - \left(\frac{I}{P} + 1\right)\right] \cdot I, \tag{5.4}$$

where N represents a number of subcarriers, P denotes nominal pilot spacing and I represents interpolation factor. On the other hand, in the case of "Random Symbols" interpolation method the length of random symbol vector is given by

$$L^{RS} = (N-1) \cdot (I-1)\,. \tag{5.5}$$

Then, the PAPR reduction problem can be described by

$$\tilde{\mathbf{c}} = \arg\min_m \{\mathrm{PAPR}\} = \arg\min_m \left\{ \frac{\max\left\{\left|\mathbf{P}_{\mathrm{addCP}}\mathbf{F}^{\mathrm{H}}_{N_{\mathrm{FFT}}}\mathbf{A}_{N_{\mathrm{FFT}}}\left(\mathbf{x}^I + \mathbf{c}^m\right)\right|^2\right\}}{\mathrm{E}\left\{\left|\mathbf{P}_{\mathrm{addCP}}\mathbf{F}^{\mathrm{H}}_{N_{\mathrm{FFT}}}\mathbf{A}_{N_{\mathrm{FFT}}}\left(\mathbf{x}^I + \mathbf{c}^m\right)\right|^2\right\}} \right\}, \tag{5.6}$$

where $m = 1, \ldots, M$ and M represents a number of iterations. Obtained random symbol set $\tilde{\mathbf{c}}$ is chosen such that the PAPR is minimized.

Die approbierte gedruckte Originalversion dieser Diplomarbeit ist an der TU Wien Bibliothek verfügbar
The approved original version of this thesis is available in print at TU Wien Bibliothek.
TU Bibliothek Your knowledge hub WIEN

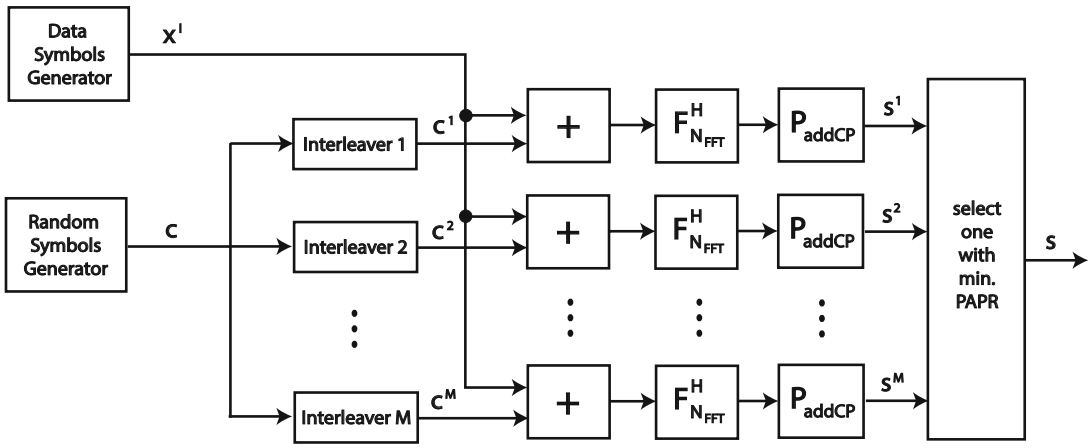

Figure 5.2: The interleaving is a technique to reduce the PAPR through permuting random symbols in a stochastic manner.

5.3.1 Interleaving

A straightforward approach to reduce the PAPR is to generate multiple random symbol blocks through interleaving. The interleaving is an operation performed at the transmitter which permutes or reorders a random symbol block in a stochastic manner [45]. The main idea of this technique is to generate a set of M different realizations by permuting random symbols in frequency-domain through a set of M different interleavers. Figure 5.2 shows a block diagram of the interleaved OFDM transmitter with employed interpolation methods.

Let us assume that the original random symbol block and one-to-one mapping operation performed by m-th interleaver are denoted by $\mathbf{c}$ and π^m, respectively. Then, the m-th permutation of random symbols $\mathbf{c}$ can be described by

$$\mathbf{c}^m = \pi^m \{\mathbf{c}\} = \left[\mathrm{c}_{\pi^m\{1\}} \quad \mathrm{c}_{\pi^m\{2\}} \quad \dots \quad \mathrm{c}_{\pi^m\{L\}}\right]^{\mathrm{T}}, \tag{5.7}$$

where $(m = 1, \dots, M)$. Thereafter, random symbols $\mathbf{c}$ are combined with data symbols $\mathbf{x}^I$ and the IDFT is performed to convert the combined signal to the time domain. Then, the PAPR of a time-domain signal $\mathbf{s}^m$ is calculated and the permutation of random symbols, which results in the lowest PAPR, is chosen to be transmitted.

To show how the interleaving technique impacts the PAPR performance, simulation is performed for both "Resample & Repeat" and "Random Symbols" interpolation methods. The simulation results are shown in Figure 5.3. Although a PAPR reduction is achieved, one can observe that the PAPR is significantly higher for the case of the "Resample & Repeat" method compared to the "Random Symbols" interpolation method.

Die approbierte gedruckte Originalversion dieser Diplomarbeit ist an der TU Wien Bibliothek verfügbar
The approved original version of this thesis is available in print at TU Wien Bibliothek.
TU Bibliothek Your knowledge hub WIEN

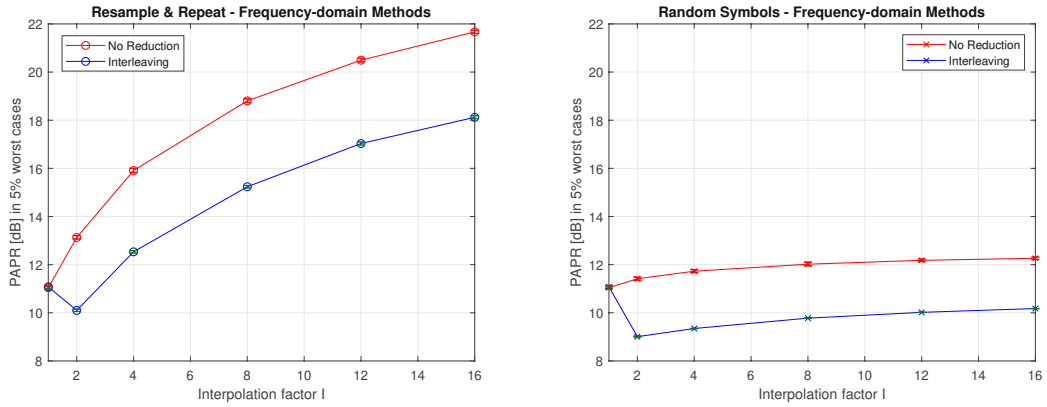

(a) (b)

Figure 5.3: The PAPR is still significantly higher for the case of the "Resample & Repeat" method compared to the "Random Symbols" interpolation method.

5.3.2 Selective Mapping

To reduce the PAPR of the "Resample & Repeat" interpolation method to a greater extent, I apply the more effective technique in terms of the PAPR reduction. More precisely, instead of interleaving once generated random symbols in the frequency domain, I perform a transformation of random symbols $\mathbf{c}$ by employing the Selective Mapping (SLM) technique. The basic idea of this technique is to generate a set of sufficiently different candidate random symbol blocks $\mathbf{c}^m$ $(m = 1, 2, \ldots, M)$ at the transmitter after the interpolation method is performed [45]. Thereafter, the random block which results in the lowest PAPR is selected for transmission. The block diagram of the SLM technique for interpolation methods is given in Figure 5.4.

Different candidate random symbol blocks $\mathbf{c}^m$ are generated by multiplying the original random block $\mathbf{c}$ with M different phase sequences $\mathbf{p}^m$ of length L, in element-by-element manner and prior to performing the IDFT [46]. This multiplication rotates original random symbols within the signal constellation. Phase sequences $\mathbf{p}^m$ can be generated such that all L phases are different and such sequence can be represented as

$$\mathbf{p}^m = \left[e^{j\varphi_1^m} \; e^{j\varphi_2^m} \; \cdots \; e^{j\varphi_L^m}\right]^T, \qquad m = 1, 2, \ldots, M, \tag{5.8}$$

where φ_l^m represents a phase shift for specific random symbol c_l. Generally, the phase shift $\varphi_{l,k}^m$ can take all values between $[0, 2\pi]$. In order to decrease the computational complexity of the transmitter, I use only two different phases ($\varphi_{l,k}^m = 0$ or $\varphi_{l,k}^m = \pi$).

Die approbierte gedruckte Originalversion dieser Diplomarbeit ist an der TU Wien Bibliothek verfügbar
The approved original version of this thesis is available in print at TU Wien Bibliothek.
TU Bibliothek Your knowledge hub WIEN

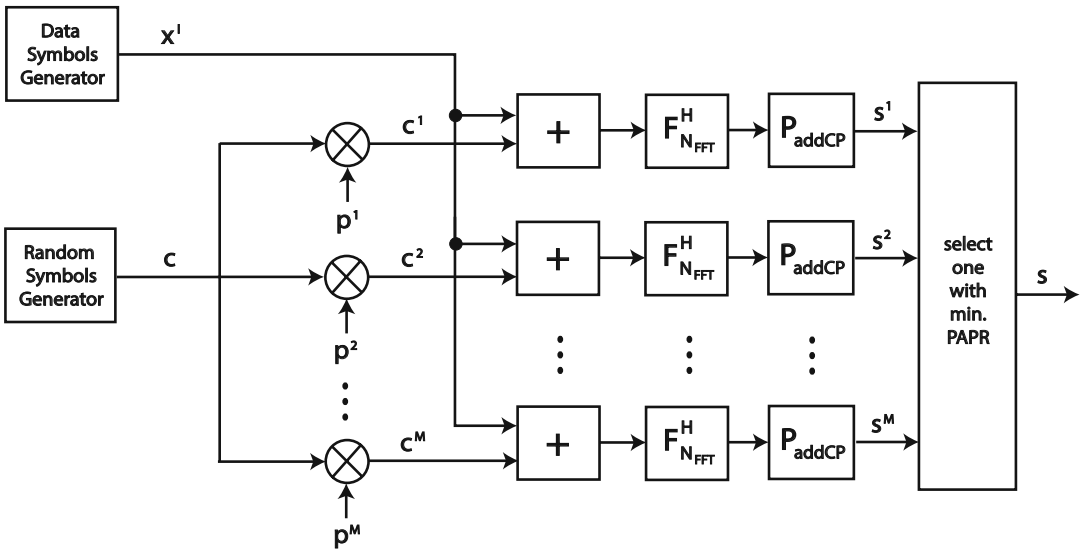

Figure 5.4: SLM generates a set of sufficiently different candidate random symbol blocks $\mathbf{c}^m$ by multiplying the original random block $\mathbf{c}$ with different phase sequences.

Hence, modified random symbol blocks $\mathbf{c}^m$ can be mathematically represented as

$$\mathbf{c}^m = \mathbf{c} \otimes \mathbf{p}^m = \left[\mathrm{c}_1 e^{j\varphi_1^m} \ \mathrm{c}_2 e^{j\varphi_2^m} \ \cdots \ \mathrm{c}_L e^{j\varphi_L^m}\right]^{\mathrm{T}}. \tag{5.9}$$

This approach is called SLM per subcarrier and requires L different phase shifts in each iteration.

To reduce the number of required phase shifts and hence the computational complexity, I propose SLM per subset approach. Such an approach is based on grouping the random symbols into different subsets, depending on the interpolation method employed and multiplying different subsets by different phases. In the case of the "Resample & Repeat" interpolation method, the number of subsets is equal to the number of signal repetitions (interpolation factor I),

$$\mathbf{c} = [\mathbf{c}_1 \ \mathbf{c}_2 \ \ldots \ \mathbf{c}_I]^T \tag{5.10}$$

and then the phase sequence can be represented as

$$\mathbf{p}^m = \left[e^{j\varphi_1^m} \ e^{j\varphi_2^m} \ \cdots \ e^{j\varphi_I^m}\right]^T, \qquad m = 1, 2, \ldots, M. \tag{5.11}$$

Hence, modified random symbol blocks $\mathbf{c}^m$ can be mathematically represented as

$$\mathbf{c}^m = \mathbf{c} \otimes \mathbf{p}^m = \left[\mathbf{c}_1 e^{j\varphi_1^m} \ \mathbf{c}_2 e^{j\varphi_2^m} \ \cdots \ \mathbf{c}_I e^{j\varphi_I^m}\right]^{\mathrm{T}}. \tag{5.12}$$

Die approbierte gedruckte Originalversion dieser Diplomarbeit ist an der TU Wien Bibliothek verfügbar
The approved original version of this thesis is available in print at TU Wien Bibliothek.
TU Bibliothek Your knowledge hub WIEN

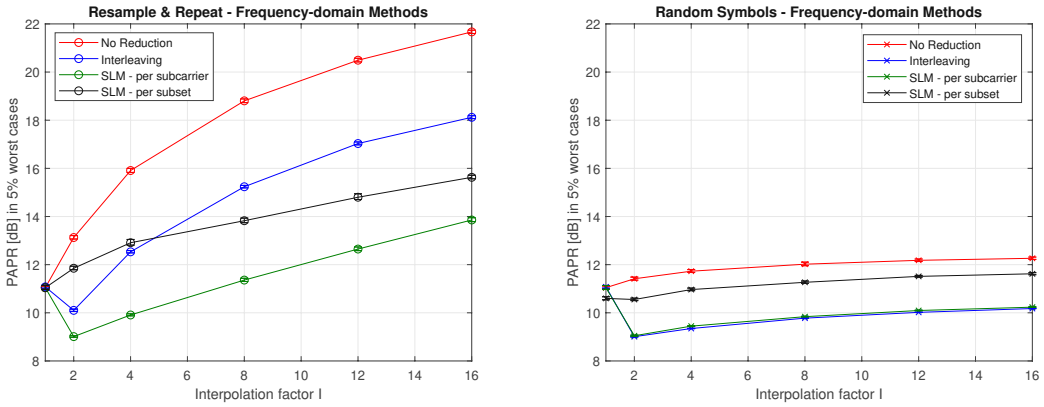

(a) (b)

Figure 5.5: SLM per subcarrier technique outperforms SLM per subset technique for both "Resample & Repeat" and "Random Symbols" interpolation methods, due to large number of phase shifts employed per each iteration.

In the case of the "Random Symbols" interpolation method, the number of subsets is equal to number of random symbol insertions between each subcarrier $(N-1)$

$$\mathbf{c} = [\mathbf{c}_1 \ \mathbf{c}_2 \ \dots \ \mathbf{c}_{N-1}]^T \tag{5.13}$$

and then the phase sequence can be described by

$$\mathbf{p}^m = \left[e^{j\varphi_1^m} \ e^{j\varphi_2^m} \ \cdots \ e^{j\varphi_{N-1}^m}\right]^T, \qquad m = 1, 2, \dots, M. \tag{5.14}$$

Hence, modified random symbol blocks $\mathbf{c}^m$ can be mathematically represented as

$$\mathbf{c}^m = \mathbf{c} \otimes \mathbf{p}^m = \left[\mathbf{c}_1 e^{j\varphi_1^m} \ \mathbf{c}_2 e^{j\varphi_2^m} \ \cdots \ \mathbf{c}_{N-1} e^{j\varphi_{N-1}^m}\right]^{\mathrm{T}}. \tag{5.15}$$

Furthermore, as described in Section 5.3, PAPR is calculated for each of these time-domain sequences and the one with the lowest PAPR is selected for transmission.

To compare SLM with the interleaving technique, the simulation-based comparison is performed for both interpolation methods. The simulation results are shown in Figure 5.5. For the case of the "Resample & Repeat" interpolation method (Figure 5.5a), both SLM techniques outperform the interleaving technique in terms of the PAPR reduction. Such an improvement in the PAPR reduction performance occurs, since random symbols are transformed (phase changed). Thereby, it is possible to counteract the effect of repetition to a greater extent. Unfortunately, this is not possible to obtain only by perturbing or interleaving, since the same random symbols remain in the signal. For the case of the "Random Symbols" interpolation method (Figure

Die approbierte gedruckte Originalversion dieser Diplomarbeit ist an der TU Wien Bibliothek verfügbar
The approved original version of this thesis is available in print at TU Wien Bibliothek.
TU Bibliothek Your knowledge hub WIEN

5.5b), it is not possible to outperform the interleaving technique, since there is no effect of repetition that the SLM can counteract. In addition, one can observe that for both "Resample & Repeat" and "Random Symbols" interpolation methods, SLM per subcarrier technique outperforms the SLM per subset technique. This outperforming occurs since the amount of achieved PAPR reduction depends on the number of different phase sequences. Since $L^{R\&R} > I$ and $L^{RS} > N - 1$, SLM per subcarrier technique shows better results in terms of the PAPR reduction. Besides depending on the number of different phase sequences, the amount of PAPR reduction increases with the number of generated phase sequences M. The drawback of the SLM per subcarrier technique lies in the fact that it is more complex than the SLM per subset technique since it requires L different phases.

5.4 Time-domain reduction methods

Frequency-domain reduction methods desrcibed in Section 5.3 require the IDFT calculation after each transformation (iteration), which increases the computational complexity of the transmitter. In order to reduce the computational complexity, I consider time-domain PAPR reduction methods which transform random symbols after the IDFT has been performed. In other words, the IDFT needs to be performed only once. Such a procedure can be described using the following notation. Let us assume that data symbols and random symbols in the frequency-domain are represented by $\mathbf{x}^I$ and $\mathbf{c}$, respectively. Thereafter, the IDFT and the CP addition are performed separately for both $\mathbf{x}^I$, given by

$$\mathbf{x}_n = \mathbf{P}_{\text{addCP}} \mathbf{F}^{\text{H}}_{N_{\text{FFT}}} \mathbf{A}_{N_{\text{FFT}}} \mathbf{x}^I \tag{5.16}$$

and $\mathbf{c}$, which is given by

$$\mathbf{c}_n = \mathbf{P}_{\text{addCP}} \mathbf{F}^{\text{H}}_{N_{\text{FFT}}} \mathbf{A}_{N_{\text{FFT}}} \mathbf{c}, \tag{5.17}$$

where $\mathbf{x}_n$ and $\mathbf{c}_n$ represent data and random symbols in the time-domain, respectively. Furthermore, $\mathbf{x}_n$ and $\mathbf{c}_n$ are summed up to obtain the time-domain transmit signal $\mathbf{s}$, described by

$$\mathbf{s} = \mathbf{x}_n + \mathbf{c}_n. \tag{5.18}$$

Then, transformation on time-domain random symbols $\mathbf{c}_n$ is performed and the PAPR of resulting signal $\mathbf{s}$ is calculated. This procedure of transformation and PAPR calculation is repeated until the minimum PAPR is found. Such PAPR reduction problem can be mathematically described by

$$\tilde{\mathbf{c}}_n = \arg\min_m \{\text{PAPR}\} = \arg\min_m \left\{ \frac{\max\left\{|\mathbf{x}_n + \mathbf{c}_n^m|^2\right\}}{\text{E}\left\{|\mathbf{x}_n + \mathbf{c}_n^m|^2\right\}} \right\}, \tag{5.19}$$

where $m = 1, \ldots, M$ and M represents the number of iterations.

Die approbierte gedruckte Originalversion dieser Diplomarbeit ist an der TU Wien Bibliothek verfügbar
The approved original version of this thesis is available in print at TU Wien Bibliothek.
TU Bibliothek Your knowledge hub WIEN

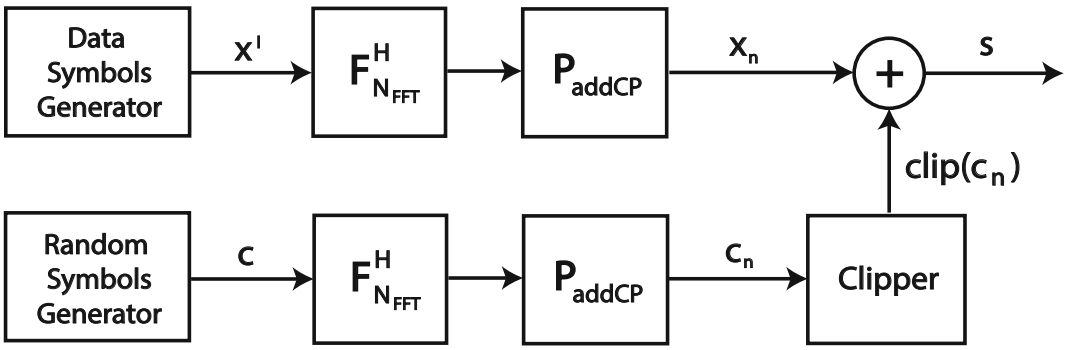

Figure 5.6: Clipping of random symbols in time-domain reduces the PAPR and avoids significant degradation of the emulation performance simultaneously.

5.4.1 Clipping and Filtering (CL)

The simplest and most widely used time-domain PAPR reduction technique is the amplitude clipping [46]. In the classical clipping approach, if the envelope of an input signal s_n exceeds pre-specified clipping level (CL), a clipper limits the envelope to that level, without changing its phase. Otherwise, the signal passes through the clipper unperturbed. In that case, the clipper can be described as

$$\mathrm{clip}\left(\mathrm{s}_n\right) = \begin{cases} \mathrm{CL}\, e^{j\phi_n}, & |\mathrm{s}_n| > \mathrm{CL} \\ \mathrm{s}_n, & |\mathrm{s}_n| \leq \mathrm{CL} \end{cases}$$

where ϕ_n is the phase of s_n. Such clipping approach will cause distortion to both data $\mathbf{x}_n$ and random signal $\mathbf{c}_n$, since the signal values above the predefined level are unknown at the receiver. Thereby, some data symbols cannot be recovered correctly. This leads to an in-band distortion which degrades Bit Error Rate (BER) performance and consequently the emulation performance of interpolation methods. Unfortunately, the in-band distortion cannot be reduced.

Therefore, I propose a modified approach of clipping and filtering technique to reduce the PAPR. In the modified clipping approach proposed in this section, if the envelope of the random signal $\mathbf{c}_n$ exceeds the pre-specified clipping level (CL), a clipper limits its envelope to that level, without changing its phase. Otherwise, the random $\mathbf{c}_n$ passes through the clipper unperturbed. This can be described as

$$\mathrm{clip}\left(\mathrm{c}_n\right) = \begin{cases} \mathrm{CL}\, e^{j\phi_n}, & |\mathrm{c}_n| > \mathrm{CL} \\ \mathrm{c}_n, & |\mathrm{c}_n| \leq \mathrm{CL} \end{cases}$$

Clipping the random signal $\mathbf{c}_n$ will produce the interference to the data signal $\mathbf{c}_n$. Since the power of such interference is significantly lower compared to the noise level,

Die approbierte gedruckte Originalversion dieser Diplomarbeit ist an der TU Wien Bibliothek verfügbar
The approved original version of this thesis is available in print at TU Wien Bibliothek.
TU Bibliothek Your knowledge hub WIEN

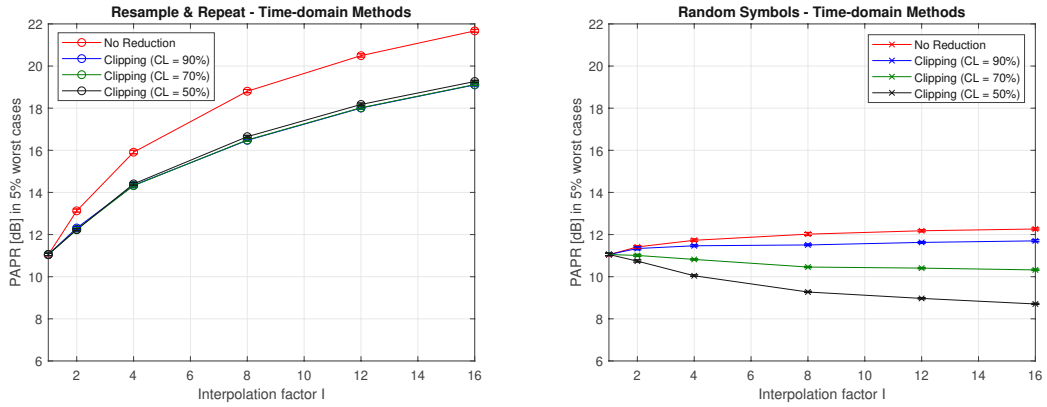

(a) (b)

Figure 5.7: The PAPR reduction increases significantly with an decreasing the CL for the case of the "Random Symbols" interpolation method, while it is not the case of the "Resample & Repeat" method.

a degradation of the BER and hence the emulation performance in practical systems is negligible. The block diagram of the proposed clipping scheme is shown in Figure 5.6.

Although the in-band distortion is avoided by using the modified approach, the clipping is a non-linear process that introduces out-of-band radiation of a multi-carrier signal [47]. The out-of-band radiation occurs, since the clipping introduces sharp changes to the signal in the time domain. This leads to out-of-band radiation, which degrades the spectral efficiency of a multi-carrier signal. Fortunately, the out-of-band radiation can be reduced by filtering the random signal after clipping. Filtering can smooth sharp signal changes introduced by clipping and hence reduce out-of-band radiation. On the other hand, filtering may also cause some peak regrowth, such that the signal after clipping and filtering will exceed the clipping level at some points [45].

In order to show how the modified clipping technique impacts the PAPR reduction performance, the simulation is performed for both "Resample & Repeat" and "Random Symbols" interpolation methods. The results of simulation for CL of 50%, 70% and 90% of $|\mathbf{c}_n|$ are shown in Figure 5.7. For the case of the "Random Symbols" interpolation method (Figure 5.7b), the PAPR reduction increases significantly with an decreasing the CL, compared to the case of the "Resample & Repeat" method. Such an effect occurs, since in the case of the "Random Symbols" method, only the number of inserted random symbols increases. On the other hand, for the case of the "Resample & Repeat" interpolation method (Figure 5.7a), decreasing the CL does not result in a significant increase of the PAPR reduction. The reason for such

Die approbierte gedruckte Originalversion dieser Diplomarbeit ist an der TU Wien Bibliothek verfügbar
The approved original version of this thesis is available in print at TU Wien Bibliothek.
TU Bibliothek Your knowledge hub WIEN

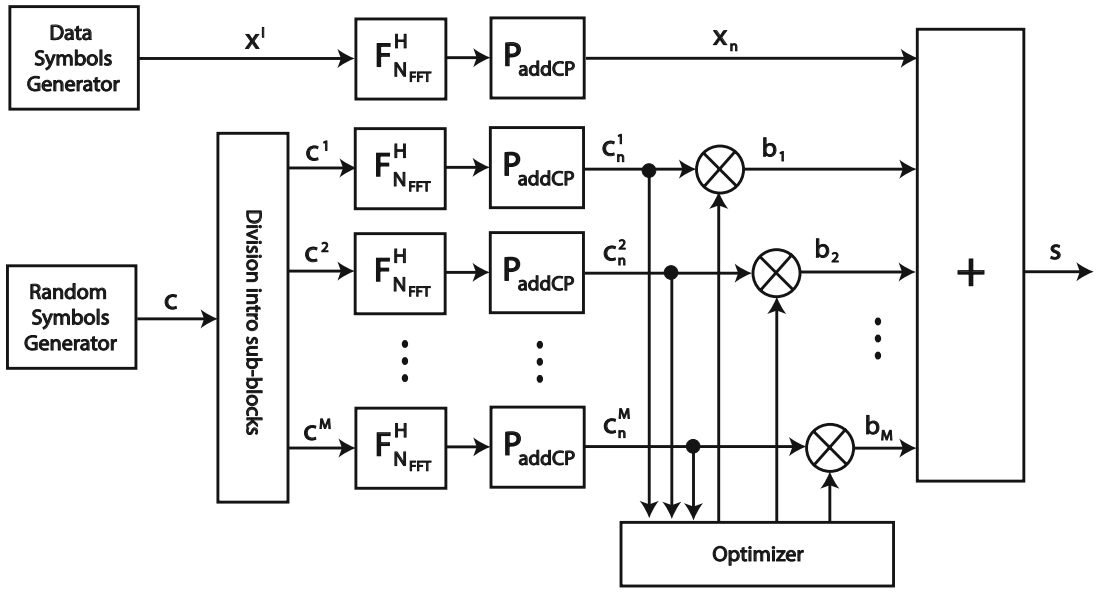

Figure 5.8: Data block $\mathbf{x}_k$ remains unchanged and random data block $\mathbf{c}_k$ of length L is partitioned into M disjoint sub-blocks.

phenomena is that clipping limits the level of random signal $\mathbf{c}_n$ without affecting its repetition property. Since the repetition property is the main cause of the large PAPR, the clipping approach does not offer a significant improvement. In this technique, the extent of PAPR reduction depends mostly on the CL employed on random symbols in the time domain.

5.4.2 Partial Transmit Sequence

Although a PAPR reduction is achieved using the clipping technique, one can observe that the PAPR is significantly higher for the case of the "Resample & Repeat" method compared to the "Random Symbols" interpolation method. Similar to frequency-domain methods, to reduce the PAPR of the "Resample & Repeat" interpolation method to a greater extent, I apply a more effective technique in terms of the PAPR reduction. More precisely, instead of clipping, I perform a transformation of the random signal $\mathbf{c}_n$ by employing the Partial Transmit Sequence (PTS) technique.

In the classical PTS approach, a time-domain signal is partitioned into M disjoint sub-blocks [30]. Thereafter, the IDFT is computed separately for each disjoint sub-block to obtain M different time-domain blocks. Each time-domain block is then multiplied by a phase factor and obtained time-domain partial transmit sequences are added together to form a transmit signal. The phase factors are

Die approbierte gedruckte Originalversion dieser Diplomarbeit ist an der TU Wien Bibliothek verfügbar
The approved original version of this thesis is available in print at TU Wien Bibliothek.
TU Bibliothek Your knowledge hub WIEN

selected such that the PAPR of the combined transmit signal is minimized. This technique is very similar to the SLM technique. The difference is that the PTS technique applies phase transformation after the IDFT, while SLM applies phase transformation before the IDFT. Therefore, some of the complexity of the several full IDFT operations can be avoided in PTS so that it is more advantageous than SLM [47].

For utilizing this technique in interpolation methods, I propose a modified version of the PTS technique. The modification is made such that input data block $\mathbf{x}^I$ remains unchanged and random data block $\mathbf{c}$ of length L is partitioned into M disjoint sub-blocks. The block diagram of the proposed PTS technique is shown in Figure 5.8. In the proposed technique, the data block $\mathbf{x}^I$ is only transformed through the IDFT and remains phase-unchanged (multiplied by the factor of 1). Considering that random symbols blocks are neglected on the receiver side, the proposed technique does not require transmitting side information about the selected phase sequence.

The partitioning of random data block $\mathbf{c}$ into M disjoint sub-blocks can be described by

$$\mathbf{c} \rightarrow \mathbf{c}^1 \ \mathbf{c}^2 \ \cdots \ \mathbf{c}^M \tag{5.20}$$

Besides disjointness, each sub-block $\mathbf{c}^m$ has to be of the length L, the same as for $\mathbf{c}$, such that all positions not containing symbols desired for specific sub-block are equal to zero. In other words, any two of these sub-blocks are orthogonal and $\mathbf{c}$ is the combination of all the M sub-blocks

$$\mathbf{c} = \sum_{m=1}^{M} \mathbf{c}^m. \tag{5.21}$$

Using the PTS technique together with proposed interpolation methods, many sub-block partitioning methods can be used. Such partitioning methods are illustrated in Figure 5.9 and can be classified into three categories:

- per insertion/repetition where random symbols from each insertion between two data symbols in the "Random Symbols" method or from each repetition in the "Resample & Repeat" method form a single sub-block
- per number where all n-th random symbols from each insertion between two data symbols in the "Random Symbols" method or from each repetition in the "Resample & Repeat" method form single sub-block
- pseudo-random where M sets of equal size are formed from randomly chosen random symbols.

Die approbierte gedruckte Originalversion dieser Diplomarbeit ist an der TU Wien Bibliothek verfügbar
The approved original version of this thesis is available in print at TU Wien Bibliothek.
TU Bibliothek Your knowledge hub WIEN

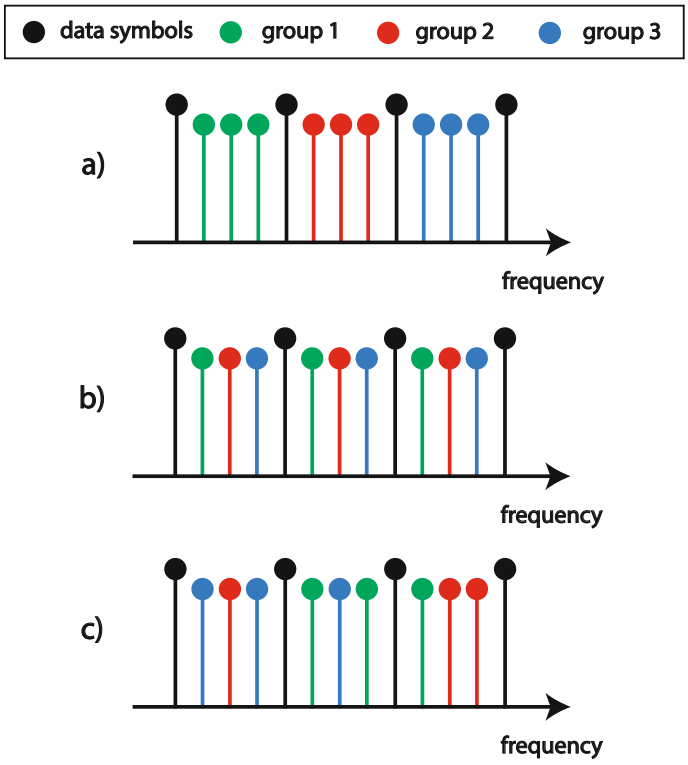

Figure 5.9: Partitioning methods can be classified into three categories: a) per insertion/repetition b) per number and c) pseudo-random

Thereafter, the IDFT is computed separately for each random symbol sub-block $\mathbf{c}^m$ as well as for the data block $\mathbf{x}^I$. Thereby, random sub-blocks $\mathbf{c}_n^m$ and the data block $\mathbf{x}_n$ in the time domain are obtained. After the IDFT, each random symbol sub-block $\mathbf{c}_n^m$ is multiplied by a phase factor $b_m = e^{j\varphi_m}$, where φ_m can take values from whole phase range $[0, 2\pi]$. The goal is to select a set of phase factors $\mathbf{b}$, such the PAPR of the transmit time-domain signal $\mathbf{s}$, defined by

$$\mathbf{s} = \mathbf{x}_n + \sum_{m=1}^{M} b_m \mathbf{c}_n^m = \mathbf{x}_n + \sum_{m=1}^{M} e^{j\varphi_m} \mathbf{c}_n^m \tag{5.22}$$

is minimized. Finding the optimum candidate requires the exhaustive search over all combinations of allowed phase factors [30]. In that case, the search complexity increases exponentially with the number of sub-blocks. In order to reduce the complexity, the search is usually limited to a small number of elements. Assume that there are W allowed phase factors to use. Then, the first phase factor b_1 can be set to 1 without any loss of performance and $M-1$ phase factors are to be found by an exhaustive search [46]. Hence, W^{M-1} sets of phase factors are searched to find the

Die approbierte gedruckte Originalversion dieser Diplomarbeit ist an der TU Wien Bibliothek verfügbar
The approved original version of this thesis is available in print at TU Wien Bibliothek.
TU Bibliothek Your knowledge hub WIEN

optimum one.

One possible algorithm to find an optimal set of phase factors b_m is proposed in [33]. Proposed combining algorithm achieves good performance with a minimal number of used phase factors ($b_m = 1$ or $b_m = -1$), in order to reduce the computational complexity. The algorithm is described by following steps:

1. Partition random symbol block $\mathbf{c}$ into M sub-blocks.
2. Set $\mathbf{b} = [1, 1, \ldots, 1]^{\mathrm{T}}$.
3. Perform the IDFT, add the CP and compute the PAPR for obtained transmit signal $\mathbf{s}$.
4. Invert the first phase factor such that $\mathbf{b} = [-1, 1, \ldots, 1]^{\mathrm{T}}$.
5. Perform the IDFT, add the CP and recompute the PAPR for obtained transmit signal $\mathbf{s}$.
6. If PAPR for $b_1 = -1$ is smaller then the PAPR for $b_1 = 1$, retain the $b_1 = -1$; otherwise set $b_1 = 1$.
7. Repeat steps 2. to 6. for each m until all phase factors have been explored.

In order to show how different partitioning methods impact the PAPR reduction performance, the simulation is performed for both interpolation methods. The simulation results are shown in Figure 5.10. For the case of the "Resample & Repeat" interpolation method (Figure 5.10a), all PTS techniques outperform the greedy clipping approach, but not in a greater extent. The reason for such phenomena is that PTS techniques affect the repetition property of resulting signal $\mathbf{s}$, which is the main cause of the large PAPR in this case. As the number of repetitions increases, its effect becomes dominant and hence there is almost no difference among clipping and the PTS techniques for a large I. On the other side, for the case of the "Random Symbols" interpolation method (Figure 5.10b), per insertion and pseudo-random PTS approach outperform the clipping, while it does not hold for per number PTS approach. In the "Random Symbols" per number PTS approach, it happens due to the small number of sub-blocks employed.

In addition, for both interpolation methods, it is possible to observe that pseudo-random partitioning outperforms the other two partitioning methods. The reason for that is the randomness which the other two methods do not pose. In the case of "Resample & Repeat" interpolation method, by using the per number

Die approbierte gedruckte Originalversion dieser Diplomarbeit ist an der TU Wien Bibliothek verfügbar
The approved original version of this thesis is available in print at TU Wien Bibliothek.
TU Bibliothek Your knowledge hub WIEN

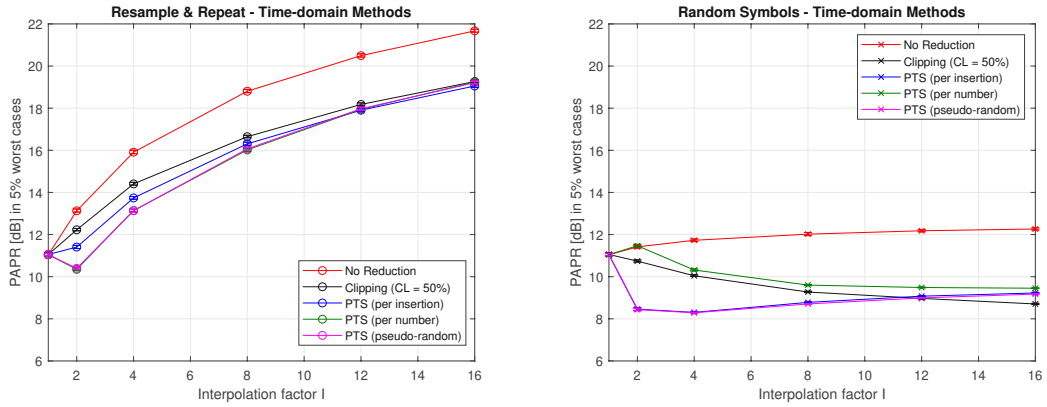

(a) (b)

Figure 5.10: Pseudo-random partitioning outperforms other two partitioning methods for both "Resample & Repeat" and "Random Symbols" interpolation methods.

partitioning method, is it possible to achieve better PAPR reduction compared to the per repetition partitioning method. It happens since for lower interpolation factors, the number of used random symbols per repetition M_{PN} (hence the number of groups) is greater than the number of repetitions M_{PR}. The results could be completely different if the number of used subcarriers is decreased.

Unlike the "Resample & Repeat" interpolation method, per insertion partitioning outperforms per number partitioning for lower I in the case of "Random Symbols" interpolation method. The reason for that is also the number of insertions, which depends on the number of subcarriers and does not change over I. Using this interpolation method, the number of used groups in per number partitioning depends on the interpolation factor ($M_{PN} = I - 1$) and consequently, the PAPR decreases with I.

5.4.3 Tone Reservation

Apart from the clipping and PTS approach, one more promising time-domain PAPR reduction technique is Tone Reservation (TR). The classical TR approach is based on the reservation of some data subcarrier subset in order to generate a PAPR reduced signal [47]. Consequently, this subcarrier subset can not be used for data transmission, which is the main drawback of this approach.

As already explained, when using proposed interpolation methods, there are already additional random subcarriers $\mathbf{c}$, which are not used for data transmission. Therefore,

Die approbierte gedruckte Originalversion dieser Diplomarbeit ist an der TU Wien Bibliothek verfügbar
The approved original version of this thesis is available in print at TU Wien Bibliothek.
TU Bibliothek Your knowledge hub WIEN

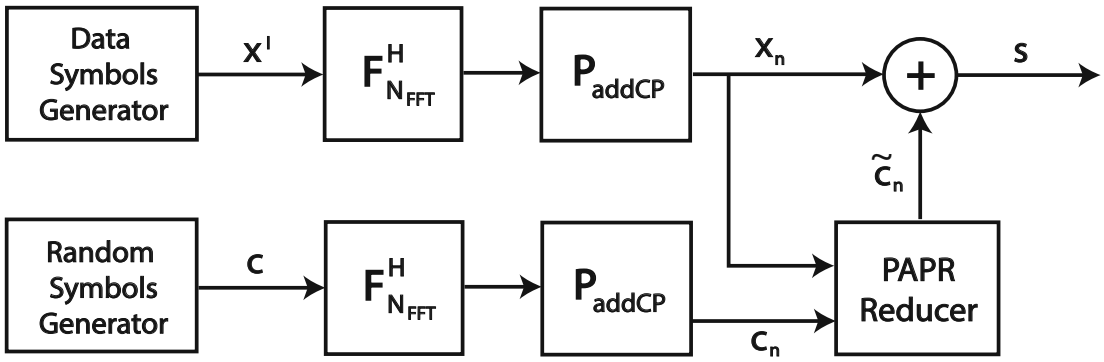

Figure 5.11: TR technique finds a proper time-domain random signal $\mathbf{c}_n$, which needs to minimize the maximum peak value of the $\mathbf{s}_n$ signal and hence to reduce the PAPR.

these subcarriers could be reserved for the PAPR reduction and hence the number of data subcarriers $\mathbf{x}^I$ remains unchanged. The same as for other time-domain PAPR reduction techniques, the IDFT is performed separately on $\mathbf{x}^I$ and $\mathbf{c}$, thereby obtaining $\mathbf{x}_n$, $\mathbf{c}_n$ and $\mathbf{s}$, which represent the data signal, the random signal and their summation in time-domain, respectively. The goal of the TR is to find a proper time-domain random signal $\mathbf{c}_n$, which needs to change the statistical distribution of the summation in the time-domain $\mathbf{s}$ and hence to reduce the PAPR [46]. More precisely, the time-domain signal $\mathbf{c}_n$ needs to minimize the maximum peak value of the $\mathbf{s}$ signal, which can be described as

$$\min_{\mathbf{c}_n} \|\mathbf{s}\|_\infty = \min_{\mathbf{c}_n} \|\mathbf{x}_n + \mathbf{c}_n\|_\infty. \tag{5.23}$$

In order to approach the optimum time-domain random signal $\mathbf{c}_n$, Tellado in [28] and Chen in [29] proposed a simple gradient iterative algorithm. The block diagram of the TR technique is depicted in Figure 5.11.

This iterative algorithm is based on the amplitude clipping and its goal is to minimize the MSE of the clipping noise. The amplitude clipping described in Section 5.4.1 introduces a noise to the time-domain signal $\mathbf{s}$, called the Clipping Noise. Then, the Clipping Noise Power (CNP) can be defined as

$$\mathrm{CNP} = \|\mathbf{s} - \mathrm{clip}\,(\mathbf{s})\,\|_2^2 \tag{5.24}$$

and the Signal-to-Clipping Noise Ratio (SCR) as

$$\mathrm{SCR} = \frac{\|\mathbf{s}\|_2^2}{\|\mathbf{s} - \mathrm{clip}\,(\mathbf{s})\,\|_2^2}. \tag{5.25}$$

If tones for peak reduction $\mathbf{c}_n$ are included, the equation (5.25) can be rewritten as

$$\mathrm{SCR} = \frac{\|\mathbf{x}_n + \mathbf{c}_n\|_2^2}{\|\mathbf{x}_n + \mathbf{c}_n - \mathrm{clip}\,(\mathbf{x}_n + \mathbf{c}_n)\,\|_2^2}. \tag{5.26}$$

Die approbierte gedruckte Originalversion dieser Diplomarbeit ist an der TU Wien Bibliothek verfügbar
The approved original version of this thesis is available in print at TU Wien Bibliothek.
TU Bibliothek Your knowledge hub WIEN

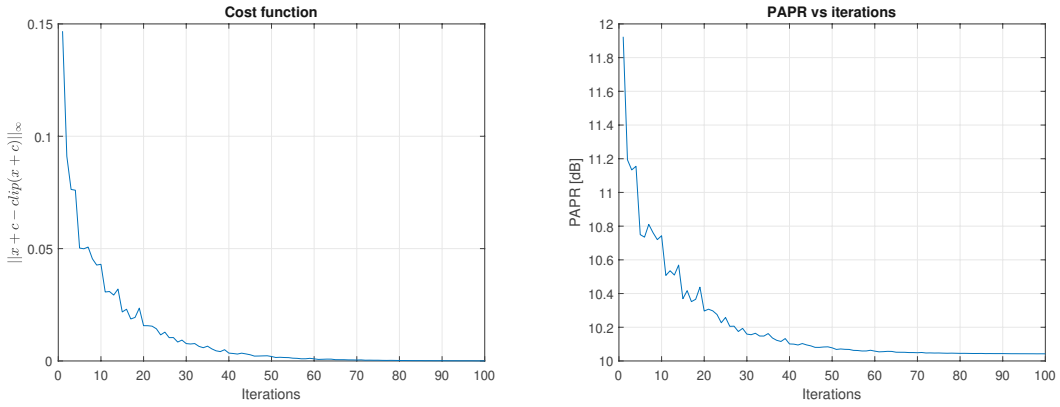

(a) (b)

Figure 5.12: The cost function $\|\mathbf{x}_n + \mathbf{c}_n - \text{clip}\left(\mathbf{x}_n + \mathbf{c}_n\right)\|_2^2$ and hence the PAPR decrease with number of iterations

Since the goal of this iterative algorithm is to minimize the MSE of the clipping noise, the SCR needs to be maximized, which can be done by minimizing its denominator. Instead of solving for $\mathbf{c}_n$ exactly, [28] and [29] describe a gradient-based iterative algorithm. Thereby, it can be shown that the gradient with respect to $\mathbf{c}_n$ of the denominator in (5.26) is

$$\nabla_{\mathbf{c}_n}\|\mathbf{x}_n + \mathbf{c}_n - \text{clip}\left(\mathbf{x}_n + \mathbf{c}_n\right)\|_2^2 = \alpha_n \mathbf{g}, \tag{5.27}$$

where $\alpha_n = \text{sign}\left(\text{x}_{n,t_m} + \text{c}_{n,t_m}\right)\left(\left|\text{x}_{n,t_m} + \text{c}_{n,t_m}\right| - \text{CL}\right)$ is a scaling factor relying on the maximum peak of $(\mathbf{x}_n + \mathbf{c}_n)$ found at t_m time-index. The constant vector $\mathbf{g}$ described by

$$\mathbf{g} = \begin{bmatrix}\text{g}_1 & \text{g}_2 & \cdots & \text{g}_{N_{\text{FFT}}}\end{bmatrix}^{\text{T}} \tag{5.28}$$

is the time-domain kernel signal used to cancel the maximum peak of $(\mathbf{x}_n + \mathbf{c}_n)$. In order to obtain optimum $\mathbf{c}_n$, the gradient based iterative algorithm updates the $\mathbf{c}_n$ with

$$\mathbf{c}_n^{(l+1)} = \mathbf{c}_n^{(l)} - \alpha_n^l \mathbf{g}_{t-t_m^l}, \tag{5.29}$$

where α_n^l and $\mathbf{g}_{t-t_m^l}$ represent a scaling factor relying on the maximum peak found at the l-th iteration and circularly shifted version of $\mathbf{g}$ to the right by a value of t_m^l, respectively. The α_n^l can be represented as

$$\alpha_n^l = \text{sign}\left(\text{x}_{n,t_m^l} + \text{c}_{n,t_m^l}^l\right)\left(\left|\text{x}_{n,t_m^l} + \text{c}_{n,t_m^l}\right| - \text{CL}\right) \tag{5.30}$$

and t_m^l is defined as

$$t_m^l = \arg\max_t \left|\text{x}_{n,t} + \text{c}_{n,t}^{(l)}\right|. \tag{5.31}$$

Die approbierte gedruckte Originalversion dieser Diplomarbeit ist an der TU Wien Bibliothek verfügbar
The approved original version of this thesis is available in print at TU Wien Bibliothek.
TU Bibliothek Your knowledge hub WIEN

One example of minimizing the cost function, which is $\|\mathbf{x}_n + \mathbf{c}_n - \mathrm{clip}\left(\mathbf{x}_n + \mathbf{c}_n\right)\|_2^2$ and the PAPR is shown in Figure 5.12. As expected, the cost function and hence the PAPR decreases with number of iterations.

In an ideal case, the time-domain kernel $\mathbf{g}$ should be a discrete impulse which needs to cancel the maximum peak of $(\mathbf{x}_n + \mathbf{c}_n)$ without affecting other signal samples at each iteration [29]. Unfortunately, such a time-domain kernel signal cannot be generated in a real case due to the finite number of tones for peak reduction. With a finite number of tones, sample values not located at maximum peak ($t \neq t_m$) could also be increased. In other words, trying to reduce the maximum peak of each iteration leads to a generation of secondary peaks. To keep secondary peaks as low as possible with a limited number of tones for peak reduction, $\mathbf{g}$ needs to be optimized beforehand.

The time-domain kernel $\mathbf{g}$ is obtained from tones for peak reduction and can be represented as [29]

$$\mathbf{g}\left(\mathbf{G}\right) \overset{\text{def}}{=} \begin{bmatrix} \mathrm{g}_1\left(\mathbf{G}\right) & \mathrm{g}_2\left(\mathbf{G}\right) & \cdots & \mathrm{g}_{N_{\mathrm{FFT}}}\left(\mathbf{G}\right) \end{bmatrix}^{\mathrm{T}} = \mathbf{F}^{\mathrm{H}}\mathbf{G}. \tag{5.32}$$

The matrix $\mathbf{G}$ expressed as

$$\mathbf{G} = \begin{bmatrix} \mathrm{G}_1 & \mathrm{G}_2 & \cdots & \mathrm{G}_L \end{bmatrix}^{\mathrm{T}} \tag{5.33}$$

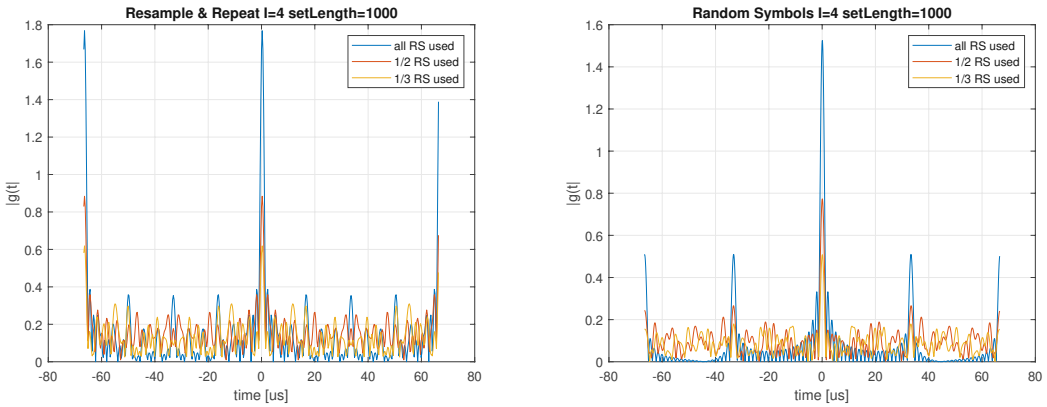

(a) (b)

Figure 5.13: In the case of "Resample & Repeat" interpolation method, apart from the main highest peak, there are also high secondary peaks. On the other hand, in the case of "Random Symbols" interpolation method, only the main highest peak occurs at $\mathrm{g}_1\left(\mathbf{G}\right)$, and secondary peaks are significantly low.

Die approbierte gedruckte Originalversion dieser Diplomarbeit ist an der TU Wien Bibliothek verfügbar
The approved original version of this thesis is available in print at TU Wien Bibliothek.
TU Bibliothek Your knowledge hub WIEN

is the frequency-domain kernel whose elements are defined as

$$\mathrm{G}_n = \begin{cases} 0, & n \in \mathcal{D} \\ 1, & n \in \mathcal{R} \end{cases}$$

where $\mathcal{D}$ and $\mathcal{R}$ denote location sets of data symbols and random symbols for PAPR reduction, respectively. Due to the properties of the IDFT, the maximum peak of $\mathbf{g}(\mathbf{G})$ is always at $\mathrm{g}_1(\mathbf{G})$. Consequently, the characteristics of $\mathbf{g}$ depend only on chosen set $\mathcal{R}$ of tones for PAPR reduction. Therefore, in order to keep secondary peaks of $\mathbf{g}$ as low as possible, it is necessary to find an optimal set $\mathcal{R}$. Consequently, the design of an optimal set $\mathcal{R}$ is a combinatorial optimization problem, which can be formulated as [29]

$$\mathbf{G}^{\star} = \arg \min_{\mathbf{G}_q \in \mathbf{\Omega}} \mathcal{C}_{\mathrm{sel}}(\mathbf{G}_q), \tag{5.34}$$

where

$$\mathcal{C}_{\mathrm{sel}}(\mathbf{G}_q) = \max\{|\mathrm{g}_2(\mathbf{G}_q)|, \ldots, |\mathrm{g}_{N_{\mathrm{FFT}}}(\mathbf{G}_q)|\}. \tag{5.35}$$

In previous equation, $\mathbf{G}^{\star}$, $\mathcal{C}_{\mathrm{sel}}(\mathbf{G}_q)$ and $\mathbf{G}_q$ represent the global optimum of the objective function, the secondary peak in $\mathbf{g}(\mathbf{G}_q)$ and the indicator of the selected subset of the feasible frequency domain kernel sequences, respectively. The matrix $\mathbf{G}_q$ is defined by

$$\mathbf{G}_q = \{I_n\}_{n=1}^{N_{\mathrm{FFT}}}, \quad I_n \in \{0,1\}, \quad q = 1, 2, \ldots, Q \tag{5.36}$$

where the indicator function I_n shows whether a reserved tone is selected at the nth position and Q represents number of possible subsets, denoted by

$$\mathbf{\Omega} = \{\mathbf{G}_1, \ldots, \mathbf{G}_Q\}. \tag{5.37}$$

To achieve the optimal selection of the set $\mathbf{G}^{\star}$, I perform a search over $\mathbf{\Omega}$ for minimizing the secondary peaks of the time-domain kernel $\mathbf{g}$. After a search, one set of random symbols with the smallest secondary peak in $\mathbf{g}$ is selected for PAPR reduction. Found sets of random symbols ($I = 4$) for cases when one-third, one-half or all random symbols have been assigned for PAPR reduction are shown in Figure 5.13. In the case of the "Resample & Repeat" interpolation method (Figure 5.13a), apart from the main highest peak at $\mathrm{g}_1(\mathbf{G})$, there are also high secondary peak at $\mathrm{g}_{\frac{N_{\mathrm{FFT}}}{2}}(\mathbf{G})$. The reason for that is the assignment of positions for random symbols in the case of the "Resample & Repeat" method. There is a minimum of one data symbol between neighboring random symbols. As a consequence, the goal of minimizing secondary peaks can not be achieved using the "Resample & Repeat" method. Thus, the TR technique can not be employed with the "Resample & Repeat" interpolation method since it is impossible to find a proper time-domain kernel. On the other hand, in the case of the "Random Symbols" interpolation method, more than one random symbols

Die approbierte gedruckte Originalversion dieser Diplomarbeit ist an der TU Wien Bibliothek verfügbar
The approved original version of this thesis is available in print at TU Wien Bibliothek.
TU Bibliothek Your knowledge hub WIEN

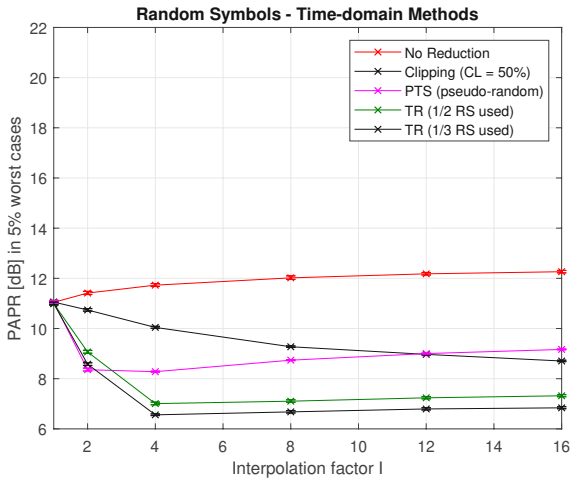

Figure 5.14: There is no significant PAPR increase with an interpolation factor I, due different assignment of random symbols for each factor.

are inserted between data symbols. Consequently, only the main highest peak occurs at $\mathrm{g}_1(\mathbf{G})$, and secondary peaks are significantly low. Therefore, the goal of minimizing secondary peaks can be achieved.

In order to show how this PAPR reduction technique impacts on "Random Symbols" interpolation method, the simulation is performed for a different number of random symbols assigned for PAPR reduction. The simulation results are shown in Figure 5.14. One can observe that the Tone Reservation technique outperforms the previously described PTS technique in terms of the PAPR reduction. When using the Tone Reservation technique, there is no significant PAPR increase with an interpolation factor I (number of additional subcarriers). It happens since for each I random symbols are differently assigned in such a manner to minimize the PAPR. In addition, the extent of PAPR reduction depends on a number of random symbols assigned for reduction. Specifically, for the OFDM system defined in Table 5.1, one-third of random symbols assigned outperform the case when one-half of random symbols are assigned for PAPR reduction.

From this analysis, I conclude that the extent of PAPR reduction in the TR technique mostly depends on the number of additional random symbols, which increases with the interpolation factor I. Besides the number of random symbols, it also depends on their locations in the frequency-domain vector $\mathbf{c}_k$ [46].

Die approbierte gedruckte Originalversion dieser Diplomarbeit ist an der TU Wien Bibliothek verfügbar
The approved original version of this thesis is available in print at TU Wien Bibliothek.
TU Bibliothek Your knowledge hub WIEN

Table 5.2: Comparison of PAPR Reduction Techniques

Technique	Domain	Reduction [dB] I=4 Resample & Repeat	Reduction [dB] I=4 Random Symbols	Complexity	Power Increase
IL	frequency	3.37	2.38	medium	no
SLM	frequency	6	2.28	medium	no
CL	time	1.5	1.68	low	no
TR	time		5.16	high	yes
PTS	time	2.77	3.44	medium	no

5.5 Simulation-based comparison

Before a specific PAPR reduction technique is chosen, many factors should be taken into consideration. These factors include PAPR reduction capability, power increase in transmit signal and computational complexity [45]. Table 5.2 summarizes these factors for different PAPR reduction techniques explained in Section 5.3 and 5.4. The most important factor in choosing a PAPR reduction technique is amount of PAPR reduction given in dB. The comparative overview of PAPR reduction for all techniques is given in Figure 5.15. The amount of PAPR reduction is obtained by subtracting the initial PAPR and the reduced PAPR of OFDM signal for each interpolation method, which

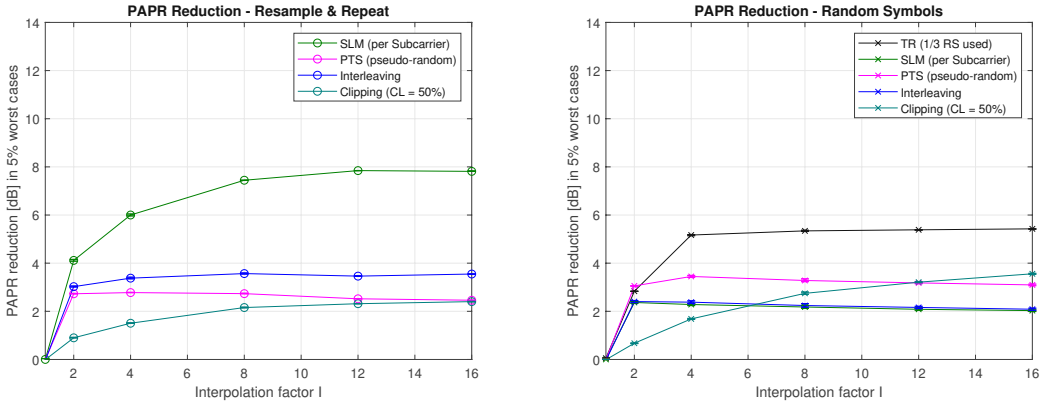

(a) (b)

Figure 5.15: The largest PAPR reduction are obtained when employing PTS technique ("Resample & Repeat" interpolation method) and TR technique ("Random Symbols" interpolation method).

Die approbierte gedruckte Originalversion dieser Diplomarbeit ist an der TU Wien Bibliothek verfügbar
The approved original version of this thesis is available in print at TU Wien Bibliothek.
TU Bibliothek Your knowledge hub WIEN

can be written as

$$\mathrm{PAPR}_{\mathrm{reduction}}[\mathrm{dB}] = \mathrm{PAPR}_{\mathrm{initial}}[\mathrm{dB}] - \mathrm{PAPR}_{\mathrm{reduced}}[\mathrm{dB}]. \tag{5.38}$$

For the case of the "Resample & Repeat" interpolation method (Figure 5.15a) the largest PAPR reduction (6 dB) is obtained when employing the SLM technique, while for the case of the "Random Symbols" (Figure 5.15b) the largest PAPR reduction is obtained, if the TR technique is employed (5.16 dB). Another important consideration in choosing a PAPR technique is computational complexity. Generally, more complex techniques have better PAPR reduction capability. In addition, frequency-domain PAPR reduction techniques are nominally more computationally complex than time-domain PAPR reduction techniques. It occurs, since frequency-domain techniques need to perform IDFT after each iteration, while time-domain techniques perform IDFT only once. Although many methods may look promising, their high computational complexity renders most of them difficult to use in practical systems. A technique with the lowest computational complexity is the Clipping and Filtering and therefore it is implemented by most commercial products. On the other side, a technique with highest computational complexity is the Tone Reservation, since it needs to find proper positions of assigned random symbols for tone reservation, before iterative algorithm. A more detailed analysis regarding the computational complexity of the PAPR reduction methods can be found in [46]. Another factor in choosing a PAPR technique is the power increase in transmit signal. Some techniques require a power increase in the transmit signal after using PAPR reduction techniques. For example, the Tone Reservation requires more signal power because some of its power must be used for the tones for PAPR reduction.

From the above described comparison, it is possible to conclude that all PAPR reduction techniques have some advantages and drawbacks. The criteria of the PAPR reduction is to find the approach that can reduce PAPR largely and at the same time it can keep the good performance in terms of the above mentioned factors as possible.

Die approbierte gedruckte Originalversion dieser Diplomarbeit ist an der TU Wien Bibliothek verfügbar
The approved original version of this thesis is available in print at TU Wien Bibliothek.
TU Bibliothek Your knowledge hub WIEN

6 6G Waveform Candidates

In this section, I provide a comparative overview of multi-carrier schemes such as Filter Bank Multi-carrier (FBMC) (Section 6.2) and Universal Filtered Multi-carrier (UFMC) (Section 6.3) proposed for use in 6G systems. After that, I provide a simulation-based comparison of proposed multi-carrier schemes in terms of power spectral density and spectral efficiency.

6.1 Motivation

Despite many advantages of OFDM modulation proposed for interpolation methods, such as low complexity and immunity to frequency-selective channels, there are also few significant drawbacks. Since OFDM uses rectangular transmit pulses, transmit symbols are then temporally disjoint which allows for low complexity implementation using IDFT/DFT and symbol-by-symbol processing. On the other hand, rectangular transmit pulses pose poor spectral decay which leads to large Out-of-Band emission (OOB). Apart from large OOB emission, OFDM poses stringent synchronization requirement and poor performance in doubly-selective HST channels. In addition, employing the cyclic prefix introduces a time overhead in the communication, resulting in a loss of spectral efficiency. To overcome such drawbacks of OFDM that lead to high inter-carrier interference (ICI), spectral efficiency degradation and poor performance in doubly-selective HST channels, the Filtered Bank Multi-carrier (FBMC) scheme is proposed for use in 6G systems as a potential successor of OFDM.

6.2 Filter Bank Multi-carrier

The FBMC scheme is based on filtering each subcarrier separately to achieve low OOB power of a particular subcarrier, as shown in Figure 6.1. In other words, the spectrum of a pulse transmitted on a single subcarrier is shaped using the transmit (synthesis) filter, which requires the application of a properly selected receiver (analysis) filter [48]. Compared to OFDM, FBMC improves the spectral efficiency of a transmission system since it does not utilize a cyclic prefix.

The principle of FBMC was first developed by Chang in 1966. Chang presented a principle of orthogonal multiplexing for transmitting pulse amplitude modulation (PAM) symbols simultaneously through a linear band-limited channel, in which ICI and ISI are eliminated by designing band-limited orthogonal signals [15]. Next, Saltzberg extended Chang's idea in [49] by employing an orthogonal multiplexed quadrature amplitude modulation (QAM) scheme.

Die approbierte gedruckte Originalversion dieser Diplomarbeit ist an der TU Wien Bibliothek verfügbar
The approved original version of this thesis is available in print at TU Wien Bibliothek.
TU Bibliothek Your knowledge hub WIEN

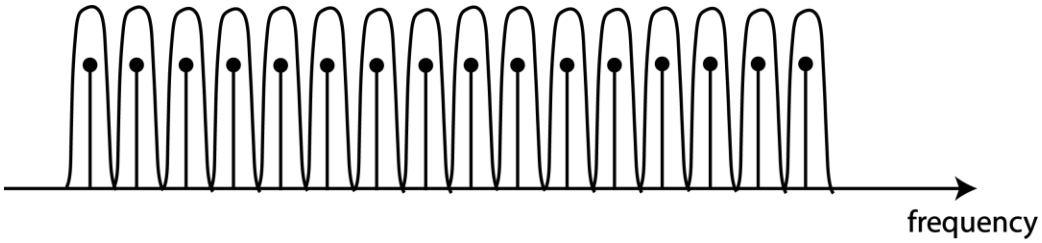

Figure 6.1: FBMC multi-carrier scheme filters each subcarrier separately to achieve low OOB power.

Considering the modulation format used, FBMC systems are classified into two groups. One group uses complex-valued QAM symbols, whereas the other group uses real-valued PAM symbols. In the case of QAM, each pulse carrying complex data is usually separated from its neighbor by $\triangle t$ in the time domain and by $2\triangle f$ in the frequency domain. Such large time-frequency spacing makes the FBMC-QAM more robust in a doubly-selective channel. On the other hand, in the case of PAM, real-valued symbols are separated from their neighbor by $\frac{\triangle t}{2}$ in the time domain and by $\triangle f$ in the frequency domain. This approach called Staggered Multi-tone (SMT) is proposed in [50]. Compared to systems applying OFDM, SMT is not orthogonal with respect to the complex plane. Consequently, each symbol introduces interference to a neighboring symbol, depending on chosen overlapping factor O [51]. This interference can be easily canceled at the receiver by introducing an offset between two neighboring symbols. Since each pair of neighboring symbols along time is treated as the real and imaginary part of the QAM symbol, this scheme is widely referred to as FBMC with Offset Quadrature Amplitude Modulation (FBMC-OQAM). In order to compare FBMC with the OFDM system in a fair manner, this thesis considers only the FBMC-OQAM scheme, because it has the same symbol density as OFDM.

FBMC transmission system relies on separate filtering of each subcarrier by means of a filter bank. The filter bank is an array of filters, which are applied to synthesize multi-carrier signals at the transmitter and analyze received signals at the receiver [52]. Filter banks employed at the transmitter and receiver are called a synthesis filter bank (SFB) and an analysis filter bank (AFB), respectively. One of the most important issues in the FBMC system is the design of the prototype filter. Generally, prototype filters are characterized by the overlapping factor O. The factor O is an integer number and represents the number of multi-carrier symbols overlapping in the time domain and the number of frequency coefficients introduced between the FFT filter coefficients in the frequency domain [53]. Such a prototype filter needs to be designed so that no ISI occurs between symbols, despite the overlapping in the time domain. Besides no ISI condition, a prototype filter needs to exhibit good time- and

Die approbierte gedruckte Originalversion dieser Diplomarbeit ist an der TU Wien Bibliothek verfügbar
The approved original version of this thesis is available in print at TU Wien Bibliothek.
TU Bibliothek Your knowledge hub WIEN

frequency-localization, obtaining a fast decay of its sidelobes in the frequency domain.

In this thesis, the design of the prototype filter is based on the Hermite pulse proposed in [54]. Such pulse is based on Hermite polynomials $H_n(\cdot)$:

$$p(t) = \frac{1}{\sqrt{\triangle t}} \mathrm{e}^{-2\pi\left(\frac{t}{\triangle t}\right)^2} \sum_{\substack{i=\{0,4,8,\\12,16,20\}}} a_i H_i\left(2\sqrt{\pi}\frac{t}{\triangle t}\right), \tag{6.1}$$

for which coefficients can be found in [55]

$$\begin{aligned} a_0 &= \quad 1.412692577 \quad a_{12} = -2.2611 \cdot 10^{-9} \\ a_4 &= -3.0145 \cdot 10^{-3} \quad a_{16} = -4.4570 \cdot 10^{-15} \\ a_8 &= -8.8041 \cdot 10^{-6} \quad a_{20} = \quad 1.8633 \cdot 10^{-16}. \end{aligned}$$

The Hermite pulse is based on a Gaussian pulse and has the same shape in time and frequency. Therefore, such pulse poses a good localization in both time and frequency. Furthermore, the good localization of the Hermite pulse causes a fast decay of its sidelobes, making it relatively robust to time- and frequency-selective channels.

The implementation of the FBMC transmission system can be described in continuous-time or discrete-time notation. Firstly, a continuous-time notation will be considered. In the FBMC transmitter, let us assume that a multi-carrier signal consisting of K data symbols is transmitted simultaneously on N different subcarriers. Such a multi-carrier signal is passed through the SFB. Thereafter, these spectrally shaped data symbols are summed up, synthesizing a composite transmit signal $s(t)$, which can be written as

$$s(t) = \sum_{k=0}^{K-1} \sum_{l=0}^{N-1} g_{n,k}(t) \mathrm{x}_{n,k}, \tag{6.2}$$

where $\mathrm{x}_{n,k}$ and $g_{n,k}(t)$ denote the transmitted data symbol on the n-th subcarrier during the k-th symbol period and transmit basis pulse, respectively. The transmit basis pulse $g_{n,k}(t)$ represents time and frequency shifted version of the transmit prototype filter $p_{TX}(t)$ and it is defined as

$$g_{n,k}(t) = p_{TX}(t - k\triangle t)\mathrm{e}^{\mathrm{j}2\pi n \triangle f (t - k\triangle t)} \mathrm{e}^{\mathrm{j}\theta_{n,k}}, \tag{6.3}$$

where $\triangle t$, $\triangle f$ and $\theta_{n,k} = \frac{\pi}{2}(n+k)$ denote the time spacing, the frequency spacing (subcarrier spacing) and phase shift, respectively [56].

The transmit signal $s(t)$ is sent through a channel and the received signal $r(t)$ is obtained at the channel output. Next, the received signal $r(t)$ is passed through the

Die approbierte gedruckte Originalversion dieser Diplomarbeit ist an der TU Wien Bibliothek verfügbar
The approved original version of this thesis is available in print at TU Wien Bibliothek.
TU Bibliothek Your knowledge hub WIEN

AFB, where each filter in the bank analyses a different subcarrier band. The receive basis filter $q_{n,k}(t)$ represents time and frequency shifted version of the receive prototype filter $p_{RX}(t)$ and can be written as

$$q_{n,k}(t) = p_{RX}(t - k\triangle t)\mathrm{e}^{-j2\pi n\triangle f(t-k\triangle t)}\mathrm{e}^{-j\theta_{n,k}}. \tag{6.4}$$

Since it is tedious to analytically calculate this continuous-time domain representation in time-varying channels, the FBMC implementation in a discrete-time domain will be introduced. Data symbols $\mathrm{x}_{n,k}$ can be represented by $\mathbf{X}$ in a matrix-form, where rows and columns represent subcarriers and symbols in time, respectively. Thereafter, matrix $\mathbf{X}$ consisting of QAM symbols is vectorized (readout column-by-column) and defined as $\mathbf{x} \in \mathbb{C}^{NK\times 1}$ vector, which is given by

$$\begin{aligned}\mathbf{x} = \mathrm{vec}\left\{\mathbf{X}\right\} &= \mathrm{vec}\left\{\begin{bmatrix} \mathrm{x}_{1,1} & \cdots & \mathrm{x}_{1,K} \\ \vdots & \ddots & \vdots \\ \mathrm{x}_{N,1} & \cdots & \mathrm{x}_{N,K}\end{bmatrix}\right\} \\ &= \begin{bmatrix}\mathrm{x}_{1,1} & \mathrm{x}_{2,1} & \cdots & \mathrm{x}_{N,1} & \mathrm{x}_{1,2} & \cdots & \mathrm{x}_{N,K}\end{bmatrix}^{\mathsf{T}}.\end{aligned}$$

Then, the basis pulses in $g_{n,k}(t)$ in (6.3) are sampled at sampling rate $f_{\mathrm{s}} = \triangle f N_{\mathrm{FFT}}$ and stacked in a basis pulse vector $\mathbf{g}_{n,k} \in \mathbb{C}^{L_{\mathrm{s}}\times 1}$ according to

$$[\mathbf{g}_{n,k}]_i = \sqrt{t_s}g_{n,k}(t)\Big|_{t=(i-1)t_s-(O-1)\triangle t}, \tag{6.5}$$

where $t_s = 1/f_s$ represents the sampling time. In (6.5) $i = 1, \ldots, L_s$, where the total number of samples is given by $L_s = ON_{\mathrm{FFT}} + \frac{N_{\mathrm{FFT}}}{2}(K-1)$. Utilizing (6.5) I define the basis pulse matrix at time position k by $\mathbf{G}_k \in \mathbb{C}^{L_{\mathrm{s}}\times N}$

$$\mathbf{G}_k = \begin{bmatrix}\mathbf{g}_{1,k} & \ldots & \mathbf{g}_{N,k}\end{bmatrix} \tag{6.6}$$

and the overall basis pulse matrix by $\mathbf{G} \in \mathbb{C}^{L_s\times NK}$

$$\begin{aligned}\mathbf{G} &= \begin{bmatrix}\mathbf{G}_1 & \ldots & \mathbf{G}_K\end{bmatrix} \\ &= \begin{bmatrix}\mathbf{g}_{1,1} & \ldots & \mathbf{g}_{N,1} & \mathbf{g}_{1,2} & \ldots & \mathbf{g}_{N,K}\end{bmatrix}\end{aligned} \tag{6.7}$$

The sampled version of the transmit signal $s(t)$ defined in (6.2) can then be described by the sampled transmit signal $\mathbf{s} \in \mathbb{C}^{L_s\times 1}$

$$\mathbf{s} = \mathbf{G}\mathbf{x}. \tag{6.8}$$

At the receiver side, after passing through a multipath time-varying channel, the received signal $\mathbf{r} \in \mathbb{C}^{L_s\times 1}$ is given by

$$\mathbf{r} = \mathbf{H}\mathbf{s} + \mathbf{n} = \mathbf{H}\mathbf{G}\mathbf{x} + \mathbf{n}, \tag{6.9}$$

Die approbierte gedruckte Originalversion dieser Diplomarbeit ist an der TU Wien Bibliothek verfügbar
The approved original version of this thesis is available in print at TU Wien Bibliothek.
TU Bibliothek Your knowledge hub WIEN

where $\mathbf{H}$ and $\mathbf{n}$ represent time-varying channel convolution matrix and additive white Gaussian noise vector.

Similar as for SFB, the AFB can be represented by, the sampled receive basis pulses $\mathbf{q}_{n,k} \in \mathbb{C}^{L_s \times 1}$. Such receive basis pulses can be stacked in a matrix $\mathbf{Q}$ according to

$$\mathbf{Q} = \begin{bmatrix} \mathbf{q}_{1,1} & \dots & \mathbf{q}_{N,1} & \mathbf{q}_{1,2} & \dots & \mathbf{q}_{N,K} \end{bmatrix}. \tag{6.10}$$

In that case, the received signal $\mathbf{r}$ is passed through AFB

$$\mathbf{y} = \mathbf{Q}^{\mathrm{H}}\mathbf{r} = \mathbf{Q}^{\mathrm{H}}\mathbf{H}\mathbf{G}\mathbf{x} + \mathbf{w}, \tag{6.11}$$

where $\mathbf{w} = \mathbf{Q}^{\mathrm{H}}\mathbf{n}$. Since the imaginary interference ($\mathbf{Q}^{\mathrm{H}}\mathbf{G} = \mathbf{I}_{NK}$) is orthogonal to the useful signal, there is no influence on the performance and it can be ignored [57]. I further assume that the channel induced interference is dominated by the noise, time-varying wireless channels are highly underspread. In other words, elements which do not lie on the main diagonal of $\mathbf{Q}^{\mathrm{H}}\mathbf{H}\mathbf{G}$ are negligible compared to the noise. Therefore, only elements on the main diagonal remain. Consequently, it is possible to write a vectorized version of received symbols $\mathbf{y} \in \mathbb{C}^{NK \times 1}$ according to

$$\mathbf{y} \approx \mathrm{Diag}\left(\mathbf{h}\right)\mathbf{Q}^{\mathrm{H}}\mathbf{G}\mathbf{x} + \mathbf{w} \tag{6.12}$$

where $\mathbf{h} \in \mathbb{C}^{NK \times 1}$ represents the one-tap channel or diagonal elements of $\mathbf{Q}^{\mathrm{H}}\mathbf{H}\mathbf{G}$. In FBMC-QAM, the orthogonality condition implies that $\mathbf{Q}^{\mathrm{H}}\mathbf{G} = \mathbf{I}_{NK}$, while in FBMC-OQAM only real orthogonality holds true, that is, $\Re\{\mathbf{Q}^{\mathrm{H}}\mathbf{G}\} = \mathbf{I}_{NK}$. Here, the operator $\Re\{\cdot\}$ takes only real part of its input. The imaginary interference in FBMC-OQAM can be canceled by phase equalization followed by taking the real part. Note that, discarding the imaginary interference does not remove any useful information in an AWGN channel [57]. Same as in OFDM, in order to remove effects induced by the multipath propagation channel and thereby to recover transmitted QAM symbols, a zero-forcing (ZF) equalizer is employed.

In theory, FBMC has many nice features, but practical system configurations render some of them unused. As explained above, the FBMC scheme is based on filtering each subcarrier separately. To avoid spectral overlapping between neighboring subcarriers, the frequency response of the prototype filter needs to be extremely tight. Thereby, the length of the prototype filter impulse response relative to the length of a single symbol is significantly increased. The need for very long impulse responses causes various issues, especially for the transmission of data in short bursts [51].

Another significant drawback of the FBMC-OQAM scheme is associated with channel estimation. By separating real-valued symbols by only $T/2$ in the time domain and

Die approbierte gedruckte Originalversion dieser Diplomarbeit ist an der TU Wien Bibliothek verfügbar
The approved original version of this thesis is available in print at TU Wien Bibliothek.
TU Bibliothek Your knowledge hub WIEN

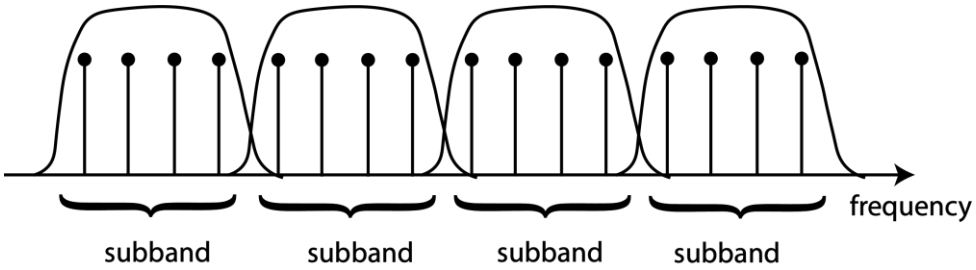

Figure 6.2: UFMC multi-carrier scheme performs block-wise filtering.

by $\triangle f$ in the frequency domain, the SMT approach causes interference between neighboring symbols. Such interference is shifted to the purely imaginary domain by $\theta_{l,k} = \frac{\pi}{2}(l+k)$ and then canceled by taking only the real part of the symbol at the receiver [58]. Unfortunately, such a simple approach cannot be used in pilot-aided channel estimation. An estimated coefficient of the wireless channel is typically complex-valued and such interference alters its imaginary part. Therefore, channel estimation of FBMC-OQAM needs a more complex approach [55] compared to a system that does not require OQAM.

6.3 Universal Filtered Multi-carrier

In order to avoid the main drawbacks of OFDM and FBMC schemes while collecting their advantages simultaneously, an alternative modulation format called the Universal Filtered Multi-carrier (UFMC) scheme has been proposed by the EU-funded research project 5GNOW [59, 60, 61] for use in 5G systems. Compared to FBMC and OFDM schemes which apply per-subcarrier filtering and filtering of the entire frequency band, respectively, the proposed UFMC scheme performs block-wise filtering. More precisely, UFMC subcarriers are divided into groups and a filtering operation is applied to a group of consecutive subcarriers, as shown in Figure 6.2.

Let us assume that N subcarriers are divided in B different sub-bands to form an UFMC symbol and that each sub-band is composed of n_i subcarriers ($N = \sum_{i=1}^{B} n_i$). Also, let us assume that K UFMC symbols are combine to form a frame. Denote now the n_i-dimensional vector ($i = 1, \ldots, B$) consisting of QAM data symbols with $(N_{\mathrm{FFT}} - N)$ zeros appended by $\tilde{\mathbf{x}}_{1,k}, \tilde{\mathbf{x}}_{2,k}, \ldots, \tilde{\mathbf{x}}_{B,k}$. In addition, denote the $(N_{\mathrm{FFT}} \times N_{\mathrm{FFT}})$ standard IDFT matrix by $\mathbf{F}^{\mathrm{H}}_{N_{\mathrm{FFT}}}$, where N_{FFT} represents FFT length. The matrix $\mathbf{F}^{\mathrm{H}}_{N_{\mathrm{FFT}}}$ can be partitioned into B submatrices $\mathbf{F}^{\mathrm{H}}_1, \mathbf{F}^{\mathrm{H}}_2, \ldots, \mathbf{F}^{\mathrm{H}}_B$ with dimensions $(N_{\mathrm{FFT}} \times n_i)$:

$$\begin{bmatrix} \mathbf{F}^{\mathrm{H}}_1 & \mathbf{F}^{\mathrm{H}}_2 & \cdots & \mathbf{F}^{\mathrm{H}}_B \end{bmatrix} \tag{6.13}$$

Die approbierte gedruckte Originalversion dieser Diplomarbeit ist an der TU Wien Bibliothek verfügbar
The approved original version of this thesis is available in print at TU Wien Bibliothek.
TU Bibliothek Your knowledge hub WIEN

The B data vectors $\tilde{\mathbf{x}}_{1,k}, \ldots, \tilde{\mathbf{x}}_{B,k}$ are transformed to time-domain by the IDFT-submatrices $\mathbf{F}_1^{\mathrm{H}}, \ldots, \mathbf{F}_B^{\mathrm{H}}$, respectively. Thereafter, the transformed data vectors are passed through filters of length L, with the possibility of using different filters for each branch. In order to perform the linear convolution by matrix-multiplication, filters are described by Toeplitz matrices $\mathbf{V}_1, \ldots, \mathbf{V}_B$, which are defined as

$$\mathbf{V}_i = \begin{bmatrix} \mathrm{v}_{i,1} & & & \\ \mathrm{v}_{i,2} & \mathrm{v}_{i,1} & & \\ \vdots & \mathrm{v}_{i,2} & \ddots & \\ \mathrm{v}_{i,L} & \vdots & \ddots & \mathrm{v}_{i,1} \\ & \mathrm{v}_{i,L} & \ddots & \mathrm{v}_{i,2} \\ & & \ddots & \vdots \\ & & & \mathrm{v}_{i,L} \end{bmatrix} \tag{6.14}$$

with dimension of $[(N_{\mathrm{FFT}} + L - 1) \times N_{\mathrm{FFT}}]$. Thereafter, filter outputs $\mathbf{s}_{1,k}, \ldots, \mathbf{s}_{B,k}$ are summed up together forming the transmit signal $\mathbf{s}_k \in \mathbb{C}^{[(N_{\mathrm{FFT}}+L-1)\times 1]}$ for k-th UFMC symbol in the frame. Whole transmit processing to obtain transmit discrete-time signal is shown in Figure 6.3 and can be mathematically expressed as

$$\mathbf{s}_k = \sum_{i=1}^{B} \mathbf{V}_i \mathbf{F}_i^{\mathrm{H}} \tilde{\mathbf{x}}_{i,k}. \tag{6.15}$$

Similar as for the FBMC, K symbols in time-domain $\mathbf{s}_k$ $(k = 1, \ldots, K)$ are vectorized

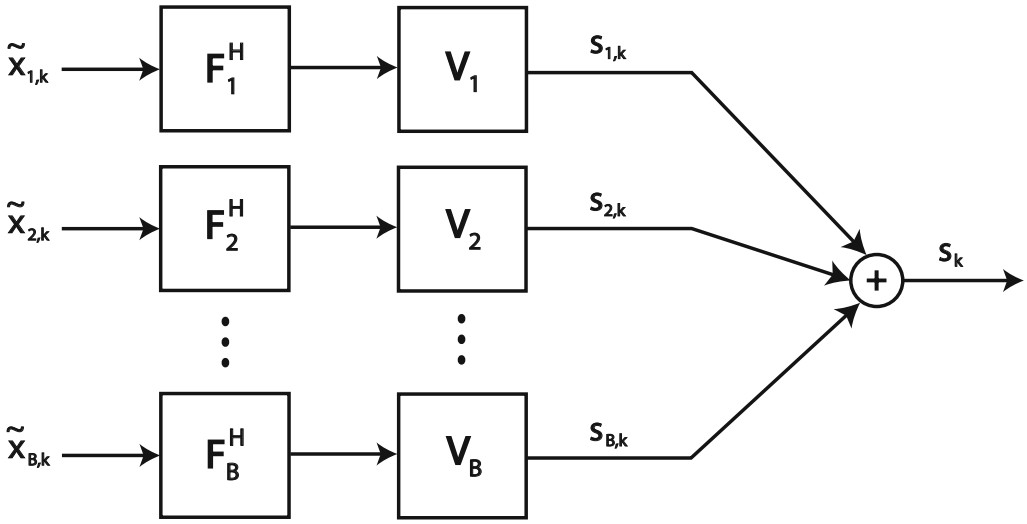

Figure 6.3: UFMC transmitter: The B data vectors are transformed to time-domain, passed through filters and summed up forming a transmit signal.

Die approbierte gedruckte Originalversion dieser Diplomarbeit ist an der TU Wien Bibliothek verfügbar
The approved original version of this thesis is available in print at TU Wien Bibliothek.
TU Bibliothek Your knowledge hub WIEN

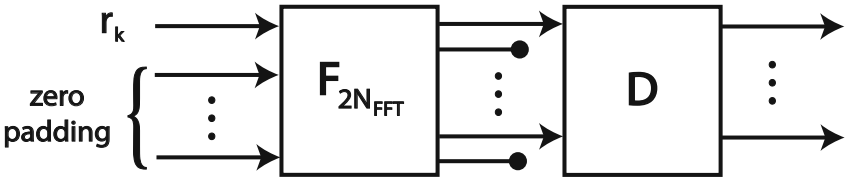

Figure 6.4: UFMC receiver: the received signal converted into the frequency domain using a $2N_{\mathrm{FFT}}$-point DFT.

to form transmit signal $\mathbf{s} \in \mathbb{C}^{L_s \times 1}$, where $L_s = (N_{\mathrm{FFT}} + L - 1) \cdot K$. Then, after passing through a multipath time-varying channel, the received signal is given by

$$\mathbf{r} = \mathbf{H}\mathbf{s} + \mathbf{n}, \tag{6.16}$$

where $\mathbf{H}$ and $\mathbf{n}$ represent time-varying channel convolution matrix and additive white Gaussian noise vector. At the receiver side, $\mathbf{r} \in \mathbb{C}^{L_s \times 1}$ is unvectorized to obtain K signals $\mathbf{r}_k \in \mathbb{C}^{(N_{\mathrm{FFT}}+L-1)\times 1}$. Thereafter, the signal is supplied to the DFT block to be converted from the time-domain into the frequency domain. As a UFMC symbol has a length of $N_{\mathrm{FFT}} + L - 1$, the conversion is performed using a $2N_{\mathrm{FFT}}$-point DFT. Thereby, missing samples at the input of the DFT block are padded with zeros [62]. After DFT transformation, non-data subcarriers are excluded from further processing. Same as in OFDM, in order to remove effects induced by the multipath propagation channel and thereby to recover transmitted QAM symbols, a zero-forcing (ZF) equalizer is employed, which result in similar complexity order as for OFDM. The whole receiver processing is shown in Figure 6.4.

The block-wise subcarrier filtering results in spectrally broader filters, compared to filters used in FBMC [51]. Consequently, such filters are shorter in time and can support the transmission of data in short bursts, which was one of the main drawbacks of FBMC. In addition, UFMC is orthogonal with respect to the complex plain and thus, it does not need to use an offset complex symbol mapping scheme, as in the FBMC case. Therefore, UFMC is a trade-off between OFDM and FBMC which combines their advantages while avoiding its main drawbacks.

6.4 Simulation-based comparison

To prove the advantages of the 6G multi-carrier schemes mentioned above regarding spectral efficiency and OOB radiation, I compared FBMC and UFMC with OFDM by means of simulation.

The employed simulation parameters are given in Table 6.1 and simulation result are shown in Figure 6.5. Figure 6.5a shows power spectral density for different multi-carrier

Die approbierte gedruckte Originalversion dieser Diplomarbeit ist an der TU Wien Bibliothek verfügbar
The approved original version of this thesis is available in print at TU Wien Bibliothek.
TU Bibliothek Your knowledge hub WIEN

Table 6.1: Simulation Parameters for 6G Waveforms

Parameter	Value
Symbol Alphabet	64-QAM
Number of Subcarriers	24
Symbols per Frame	14
Carrier Frequency	2.5 GHz
Number of Realizations	500
Sampling Rate	15.36 MHz
FFT Size	1024
Bandwidth	360 kHz
Receiver Velocity	200 km/h
Channel Model	PedestrianB
Channel Doppler Model	Jakes

schemes. As expected, due to the usage of rectangular transmit pulses, OFDM poses poor power spectral decay which leads to large OOB radiation. By employing the FBMC scheme, which is based on filtering each subcarrier separately, the OOB radiation can be significantly reduced. Besides reduced OOB radiation, FBMC improves the spectral efficiency of a transmission system since it does not utilize the cyclic prefix (Figure 6.5b). On the other hand, as explained in Section 6.2, FBMC poses challenges in practical system configurations, such as channel estimation and transmission of data

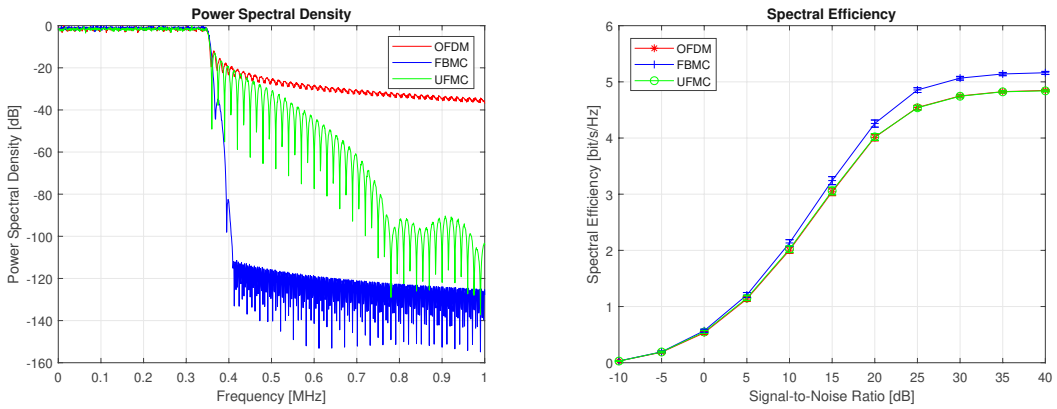

(a) (b)

Figure 6.5: FBMC und UFMC multi-carrier schemes reduce the OOB radiation and increase the spectral efficiency.

Die approbierte gedruckte Originalversion dieser Diplomarbeit ist an der TU Wien Bibliothek verfügbar
The approved original version of this thesis is available in print at TU Wien Bibliothek.
TU Bibliothek Your knowledge hub WIEN

in short bursts. A possible trade-off solution between OFDM and FBMC is UFMC scheme, which applies a filtering per-subblock basis. Such filtering decreases the OOB radiation compared to OFDM while avoiding the above explained main drawbacks of FBMC.

Die approbierte gedruckte Originalversion dieser Diplomarbeit ist an der TU Wien Bibliothek verfügbar
The approved original version of this thesis is available in print at TU Wien Bibliothek.
TU Bibliothek Your knowledge hub WIEN

7 Simulation-based validation

This section provides a more general simulation study in terms of the Signal-to-Interference Ratio (SIR) and the physical layer throughput. Firstly, I show how PAPR reduction methods and adapted channel estimation scheme proposed in Sections 4 and 5, respectively, impact the whole transmission system performance. Thereafter, I apply interpolation methods proposed in Section 3 on Filter Bank Multi-carrier (FBMC) and Universal Filtered Multi-carrier (UFMC) schemes and evaluate their HST emulation performance.

7.1 Motivation

Section 5 presented different frequency-domain and time-domain techniques to reduce the PAPR for the proposed interpolation methods. In Section 5, proposed techniques are compared in terms of the PAPR reduction capability, the power increase and the computational complexity. To use PAPR reduction techniques in practical systems, it is important to show how proposed techniques impact the power amplifier and hence the whole transmission system performance.

To compare the "Resample and Repeat" method with the original system without an interpolation method employed, Section 4 presented the adapted pilot-based channel estimation scheme. In Section 4, the proposed scheme is validated in terms of the channel MSE. In addition to the validation in terms of the channel MSE, it is important to show how the proposed channel estimation scheme impacts the whole transmission system performance.

Section 6 presented the advantages of 6G waveforms, such as the FBMC and the UFMC, over the conventional OFDM scheme, in terms of OOB radiation and spectral efficiency. Also, it is important to point out that the FBMC and the UFMC schemes employ different types of subcarrier filtering compared to the OFDM scheme. Therefore, the question arises as to whether it is possible to employ interpolation methods described in Section 3 on the FBMC and the UFMC schemes. More precisely, it is necessary to investigate whether a different type of filtering employed on the transmitter (per the whole band, per sub-band, or per subcarrier) impacts the emulation performance of proposed interpolation methods.

7.2 Peak-to-Average Power Ratio Reduction

To show how the PAPR reduction impacts the communication system performance, I performed a simulation-based comparison of OFDM signals employing the "Random Symbols" interpolation method ($I = 4$) in terms of the physical layer throughput.

Die approbierte gedruckte Originalversion dieser Diplomarbeit ist an der TU Wien Bibliothek verfügbar
The approved original version of this thesis is available in print at TU Wien Bibliothek.
TU Bibliothek Your knowledge hub WIEN

Table 7.1: Simulation Parameters for Non-linearity Test

Parameter	Value
Output Transmit Power	14:0.25:20 dBm
1-dB Compression Point	28 dBm
Saturation Power	29 dBm
Smoothness Factor	1
Modulation Format	16-QAM
Channel Coding	Turbo Code
Code Rate	616/1024
PAPR Reduction Technique	Tone Reservation
Receiver Velocity	0 km/h
Interpolation Factor	4
Number of Subcarriers	24
Symbols per Frame	14
Carrier Frequency	2.5 GHz
Number of Realizations	1000
Sampling Rate	1.92 MHz
FFT Size	256
Bandwidth	180 kHz

The comparison is performed between an OFDM signal that does not use the PAPR reduction and an OFDM signal that employs the TR technique. More precisely, I apply the non-linearity for different average output transmit power levels on both OFDM signals, to show the impact of the PAPR reduction. The non-linearity is applied according to the Rapp model given in [63] and the used power amplifier is Analog Devices HMC994AMP5E. At the receiver, the average physical layer throughput is calculated as the average over all channel realizations r and for parameters given in Table 7.1

$$D(P_t) = \frac{1}{R} \sum_{r=1}^{R} D_r(P_t), \tag{7.1}$$

where P_t and D represent the average output transmit power and the throughput, respectively.

Furthermore, I consider the "noise-free" transmission system, which is only limited by interference. Simulation results are given in Figure 7.1. If the power amplifier operates in the linear region (up to 15 dBm), there is no difference between implemented and unimplemented PAPR reduction techniques in terms of the throughput. On the other

Die approbierte gedruckte Originalversion dieser Diplomarbeit ist an der TU Wien Bibliothek verfügbar
The approved original version of this thesis is available in print at TU Wien Bibliothek.
TU Bibliothek Your knowledge hub WIEN

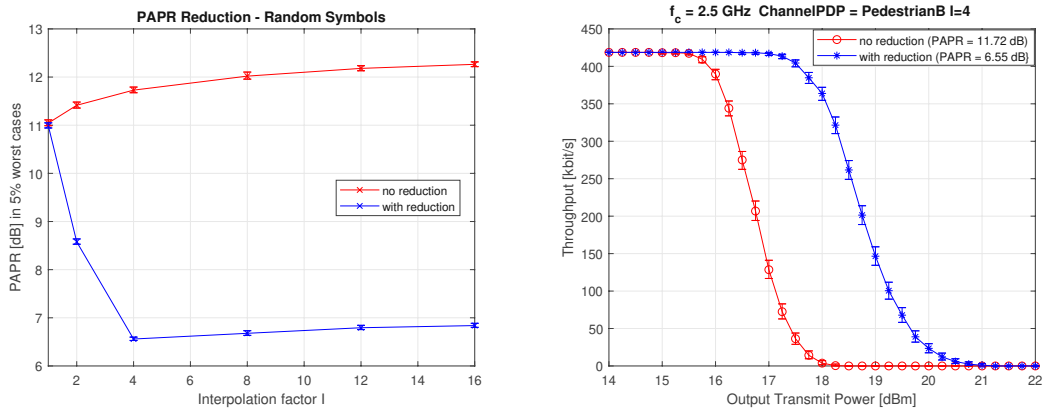

(a) (b)

Figure 7.1: PAPR reduction technique allows for the throughput to achieve higher value for the same level of the output transmit power.

hand, if the power amplifier operates near the non-linear region (from 15 dBm), one can observe the difference. In that case, although the mean signal amplitude lies within the power amplifier's linear operating region, high signal peaks fall into the non-linear region. Due to effects that occur in the non-linear region, the throughput starts to decrease with increasing the average output transmit power level. If the PAPR reduction technique is not employed, the throughput starts to decrease for a lower power output level. On the other hand, if the PAPR reduction technique is employed, such a decrease occurs for a higher level of the output transmit power. That means, by employing the PAPR reduction technique, one can achieve significantly higher throughput for the same level of the average transmit power.

7.3 Channel Estimation

To prove the applicability of the adapted channel estimation scheme, I perform different simulations in time-varying channels using the Vienna 5G Link Level Simulator [19, 20]. As a comparison reference, I use an OFDM waveform transmitted over a time-varying channel as the receiver moves at actual velocities of $v = 50, 100, 200$ and 400 km/h. This comparison reference intends to show the signal behavior in the real wireless channel. Then, interpolated versions of OFDM signals are transmitted as the receiver moves at the actual velocity of $v = 50$ km/h to emulate transmissions at $v = 100, 200$ and 400 km/h. These emulated velocities correspond to interpolation factors of $I = 2, 4$ and 8. At the receiver, the physical layer throughput is calculated. The used simulation parameters are given in Table 7.2.

Die approbierte gedruckte Originalversion dieser Diplomarbeit ist an der TU Wien Bibliothek verfügbar
The approved original version of this thesis is available in print at TU Wien Bibliothek.
TU Bibliothek Your knowledge hub WIEN

Parameter	Value
Number of Subcarriers	52
Symbols per Frame	14
Carrier Frequency	2.5 GHz
Number of Realizations	1000
Sampling Rate	10.24 MHz
FFT Size	512
Bandwidth	2.56 MHz
Channel Model	PedestrianB
Doppler Model	Jakes

Table 7.2: Simulation Parameters

Parameter	Value		
Alphabet	QAM	QAM	QAM
Modulation	4	16	64
Format			
Code Rate	78	378	466
(· 1024)	120	490	567
	193	616	666
	308		772
	449		873
	602		948

Table 7.3: MCS Parameters

For the calculation of the physical layer throughput, I used a brute-force approach where all possible Modulation and Coding Schemes (MCSs) (given in Table 7.3) are transmitted over the same channel realization and the best performing MCS in terms of data rate is chosen [14]. The used channel code is the Turbo-code. The average physical layer throughput is then calculated as the average over all channel realizations r of the data rate of the respectively best performing MCS to

$$D(v,\ I) = \frac{I}{R} \sum_{r=1}^{R} \max_{\text{MCS}} D_r(v, I, \text{MCS}), \tag{7.2}$$

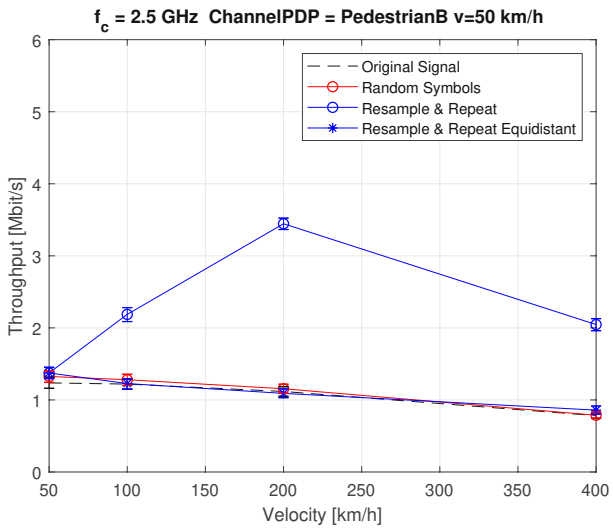

Figure 7.2: By using adapted pilot-based channel estimation scheme the "Resample & Repeat" interpolation method can be compared with the original system without an interpolation method employed.

Die approbierte gedruckte Originalversion dieser Diplomarbeit ist an der TU Wien Bibliothek verfügbar
The approved original version of this thesis is available in print at TU Wien Bibliothek.
TU Bibliothek Your knowledge hub WIEN

where D represents the throughput. In order to compare the emulated throughput rather than the actual throughput, the actual throughput is scaled with interpolation factor I as the symbol length increases with I and therefore, the throughput decreases.

Simulation results in terms of the throughput are shown in Figure 7.2. For the "Random Symbols" interpolation method, the original pilot spacing is preserved and consequently, there is no difference in the throughput when compared with the comparison reference without interpolation methods employed. In the case of "Resample & Repeat" interpolation method, when pilot-scheme with decreased pilot spacing is employed, one can observe that the throughput increases with the velocity. As explained in Section 4, it occurs due to the larger number and more dense distribution of pilot symbols in the frequency domain. On the other hand, when using the adapted pilot-based channel estimation scheme with equidistant pilot spacing, the throughput coincides with its desired comparison reference, simulated for actual receiver velocity.

7.4 6G Waveform Candidates

To show whether 6G waveform candidates can be used with "Resample & Repeat" and "Random Symbols" interpolation methods, I perform different simulations in time-varying channels according to the procedure explained in Section 7.3. In addition to the OFDM, I employ 6G waveform candidates, such as the FBMC and the UFMC. At the receiver, the Signal-to-Interference Ratio (SIR) and the physical layer throughput are calculated. I assume that the CSI is known at the receiver. The used simulation parameters are given in Table 7.4.

Table 7.4: Simulation Parameters (6G Waveforms)

Parameter	Value
Number of Subcarriers	128
Symbols per Frame	14
Carrier Frequency	2.5 GHz
Number of Realizations	500
Sampling Rate	7.68 MHz
FFT Size	1024
Bandwidth	960 kHz
Receiver Velocity	50 km/h
Channel Model	PedestrianB
Channel Doppler Model	Jakes

Die approbierte gedruckte Originalversion dieser Diplomarbeit ist an der TU Wien Bibliothek verfügbar
The approved original version of this thesis is available in print at TU Wien Bibliothek.
TU Bibliothek Your knowledge hub WIEN

The SIR is defined as the ratio of data signal power P_S and interference power P_I. In this comparison, the SIR is used to characterize the amount of ICI. The major challenge for the SIR calculation is to find an efficient way to separate the data signal and interference. I use a method that estimates SIR by separating the previously estimated interference power from the signal power containing both data signal and interference while neglecting the noise power. In other words, data signal power P_S is obtained by subtracting the interference power P_I from signal-and-interference power P_{SI}. For such estimation of the SIR, the interference power P_I needs to be known. In order to estimate the interference power P_I, subcarriers that are not too close to each other and not too close to the spectral edges are set to zero at the transmitter. Thereafter, the P_I is estimated by obtaining the power at the zero subcarrier positions $\mathcal{Z}$. On the other side, the P_{SI} is estimated from the power at non-zero data subcarrier positions $\mathcal{D}$. The SIR is then obtained as

$$\mathrm{SIR}(v,I) = \frac{\overline{P}_{SI} - \overline{P}_I}{\overline{P}_I} = \frac{\overline{P}_{SI}}{\overline{P}_I} - 1 = \frac{\frac{1}{|\mathcal{D}|}\sum_{r=1}^{R}\sum_{k=1}^{K}\sum_{n\in D}|\hat{\mathrm{x}}_{n,k,r}(v,I)|^2}{\frac{1}{|\mathcal{Z}|}\sum_{r=1}^{R}\sum_{k=1}^{K}\sum_{n\in Z}|\hat{\mathrm{x}}_{n,k,r}(v,I)|^2} - 1, \tag{7.3}$$

where $\hat{\mathrm{x}}_{n,k,r}$ represents the received symbol after the DFT in the demodulator at subcarrier n, time symbol k and channel realization r.

Simulation results for estimated SIR are shown in Figure 7.3a. As can be noticed,

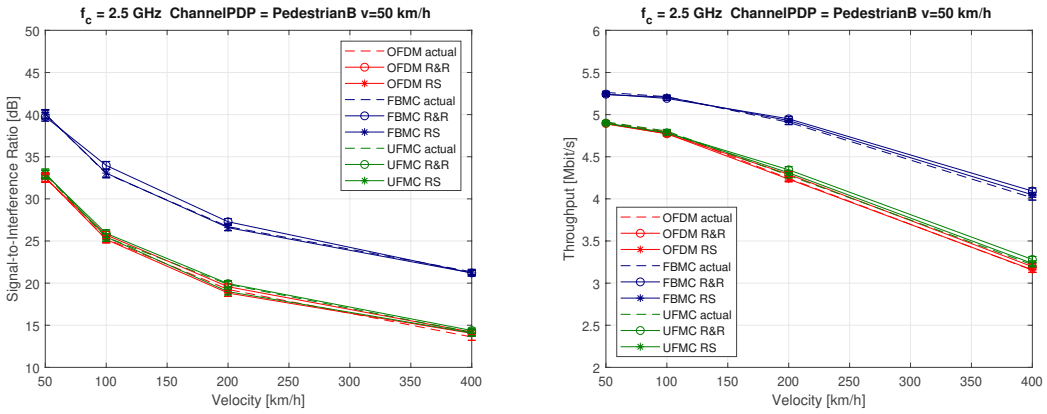

(a) (b)

Figure 7.3: The performance in terms of SIR and the throughput for both "Resample & Repeat" and "Random Symbols" interpolation methods when implemented on OFDM, FBMC and UFMC waveforms coincide with its desired comparison reference, simulated for actual receiver velocity.

Die approbierte gedruckte Originalversion dieser Diplomarbeit ist an der TU Wien Bibliothek verfügbar
The approved original version of this thesis is available in print at TU Wien Bibliothek.

both "Resample & Repeat" and "Random Symbols" interpolation methods when implemented on OFDM, FBMC and UFMC waveforms coincide with its desired comparison reference, simulated for actual receiver velocity. It is possible to conclude that type of filtering employed on the transmitter (per the whole band, per sub-band, or per subcarrier) does not impact the emulation performance of proposed interpolation methods.

Besides the SIR, the physical layer throughput is calculated at the receiver as a metric for the applicability of the different waveforms to emulate higher velocities at lower velocities. The calculation of the physical layer throughput is explained in Section 7.3. Simulation results in terms of the throughput are shown in Figure 7.3b. Same as in the case of SIR, calculated physical layer throughput for both "Resample & Repeat" and "Random Symbols" interpolation methods when implemented on OFDM, FBMC and UFMC waveforms coincide with its desired comparison reference, simulated for actual receiver velocity.

Die approbierte gedruckte Originalversion dieser Diplomarbeit ist an der TU Wien Bibliothek verfügbar
The approved original version of this thesis is available in print at TU Wien Bibliothek.
TU Bibliothek Your knowledge hub WIEN

Die approbierte gedruckte Originalversion dieser Diplomarbeit ist an der TU Wien Bibliothek verfügbar
The approved original version of this thesis is available in print at TU Wien Bibliothek.

8 Conclusion

Future railway communications systems will have to support various services to facilitate and secure the train operation, as well as to provide Internet access at high data rates to passengers. To perform performance evaluation of future railway communication systems, channel measurements in high speed scenarios need to be performed. Due to the high costs, time consumption and complexity, performing such measurements is very challenging. As a possible solution to overcome these problems, various high-speed emulation techniques have been proposed. These techniques induce effects caused by highly time-varying channels while conducting measurements at much lower speeds.

Proposed techniques to emulate high-speed effects pose an auxiliary unwanted channel estimation side effect. Such an effect leads to unequal channel estimation quality between resampling- and insertion-based time-stretching techniques. As a consequence, proposed techniques can not be compared in a fair manner. I proposed a novel channel estimation method. I conclude that channel estimation in time-interpolation methods is independent of the interpolation factor when done according to my proposed scheme. Interpolation methods with channel estimation therefore lead to the correct (comparable to the original system) performance.

Apart from the unwanted channel estimation side effect, proposed emulation techniques pose a significant increase in PAPR, making their use in real systems very challenging. Furthermore, increased PAPR limits the choice of the power amplifier at the transmitter, which results in degradation of whole system performance. In order to alleviate an increased PAPR, I adapt proposed PAPR reduction methods within time-stretching techniques, such that they can be used with more efficient power amplifiers in practical communication systems. I conclude that PAPR reduction methods in interpolation methods lead to a significant improvement of the overall system performance. Since I apply these reduction methods only on symbols that are introduced in the interpolated system, the system performance is not altered.

Proposed techniques to emulate high-speed effects have been validated for the OFDM multi-carrier scheme. Such a scheme poses low spectral efficiency, large OOB emissions, stringent synchronization requirement and poor performance in doubly-selective channels. Hence, the OFDM scheme can not meet the conditions required for future railway communications systems in high-mobility scenarios. An efficient alternative to the OFDM are FBMC and UFMC. These multi-carrier schemes are proposed for the 6G wireless communication system and employ a different type of filtering at the transmitter. Therefore, these multi-carrier schemes pose much better spectral properties than the OFDM. I validated proposed time-stretching

Die approbierte gedruckte Originalversion dieser Diplomarbeit ist an der TU Wien Bibliothek verfügbar
The approved original version of this thesis is available in print at TU Wien Bibliothek.
TU Bibliothek Your knowledge hub WIEN

techniques by using advanced 6G multi-carrier schemes, the FBMC and the UFMC. The emulation performance of both the FBMC and the UFMC coincide with the emulation performance of the OFDM. Therefore, I conclude that interpolation methods are applicable to multi-carrier schemes with different filtering approaches compared to the OFDM such as the FBMC and the UFMC.

Die approbierte gedruckte Originalversion dieser Diplomarbeit ist an der TU Wien Bibliothek verfügbar
The approved original version of this thesis is available in print at TU Wien Bibliothek.
TU Bibliothek Your knowledge hub WIEN

List of Figures

Die approbierte gedruckte Originalversion dieser Diplomarbeit ist an der TU Wien Bibliothek verfügbar
The approved original version of this thesis is available in print at TU Wien Bibliothek.
TU Bibliothek Your knowledge hub WIEN

Die approbierte gedruckte Originalversion dieser Diplomarbeit ist an der TU Wien Bibliothek verfügbar
The approved original version of this thesis is available in print at TU Wien Bibliothek.
TU Bibliothek Your knowledge hub WIEN

Die approbierte gedruckte Originalversion dieser Diplomarbeit ist an der TU Wien Bibliothek verfügbar
The approved original version of this thesis is available in print at TU Wien Bibliothek.

Die approbierte gedruckte Originalversion dieser Diplomarbeit ist an der TU Wien Bibliothek verfügbar
The approved original version of this thesis is available in print at TU Wien Bibliothek.

List of Tables

Die approbierte gedruckte Originalversion dieser Diplomarbeit ist an der TU Wien Bibliothek verfügbar
The approved original version of this thesis is available in print at TU Wien Bibliothek.

Die approbierte gedruckte Originalversion dieser Diplomarbeit ist an der TU Wien Bibliothek verfügbar
The approved original version of this thesis is available in print at TU Wien Bibliothek.

References

[1] D. He, B. Ai, K. Guan, Z. Zhong, B. Hui, J. Kim, H. Chung, and I. Kim. Channel measurement, simulation, and analysis for high-speed railway communications in 5G Millimeter-Wave band. *IEEE Transactions on Intelligent Transportation Systems*, 19(10):3144–3158, 2018.

[2] B. Ai, A. F. Molisch, M. Rupp, and Z. D. Zhong. 5G key technologies for smart railways. *Proceedings of the IEEE*, 108(6):856–893, 2020.

[3] B. Ai, X. Cheng, T. Kürner, Z. Zhong, K. Guan, R. He, L. Xiong, D. W. Matolak, D. G. Michelson, and C. Briso-Rodriguez. Challenges toward wireless communications for high-speed railway. *IEEE Transactions on Intelligent Transportation Systems*, 15(5):2143–2158, 2014.

[4] J. Wu and P. Fan. A survey on high mobility wireless communications: Challenges, opportunities and solutions. *IEEE Access*, 4:450–476, 2016.

[5] P. Unterhuber, S. Sand, M. Soliman, B. Siebler, A. Lehner, T. Strang, M. d'Atri, F. Tavano, and D. Gera. Wide band propagation in train-to-train scenarios — measurement campaign and first results. In *2017 11th European Conference on Antennas and Propagation (EUCAP)*, pages 3356–3360, 2017.

[6] J. Rodríguez-Piñeiro, J. A. García-Naya, P. Suárez-Casal, C. Briso-Rodríguez, J. I. Alonso-Montes, and L. Castedo. Assessment of channel propagation conditions for FDD LTE transmissions in the spanish high-speed railways. In *2016 10th European Conference on Antennas and Propagation (EuCAP)*, pages 1–5, 2016.

[7] R. Zhao, M. Wu, X. Xiang, and J. Yang. Measurement and modeling of the LTE train-ground channel for high-speed railway in viaduct scenario. In *2014 IEEE 80th Vehicular Technology Conference (VTC2014-Fall)*, pages 1–5, 2014.

[8] M. Alasali, C. Beckman, and M. Karlsson. Providing internet to trains using MIMO in LTE networks. In *2014 International Conference on Connected Vehicles and Expo (ICCVE)*, pages 810–814, 2014.

[9] J. Kim, M. Schmieder, M. Peter, H. Chung, S. Choi, I. Kim, and Y. Han. A comprehensive study on mmwave-based mobile hotspot network system for high-speed train communications. *IEEE Transactions on Vehicular Technology*, 68(3):2087–2101, 2019.

[10] J. Park, J. Lee, K. Kim, and M. Kim. 28-GHz high-speed train measurements and propagation characteristics analysis. In *2020 14th European Conference on Antennas and Propagation (EuCAP)*, pages 1–5, 2020.

Die approbierte gedruckte Originalversion dieser Diplomarbeit ist an der TU Wien Bibliothek verfügbar
The approved original version of this thesis is available in print at TU Wien Bibliothek.
TU Bibliothek Your knowledge hub WIEN

[11] J. Rodríguez-Piñeiro, P. Suárez-Casal, J. A. García-Naya, L. Castedo, C. Briso-Rodríguez, and J. I. Alonso-Montes. Experimental validation of ICI-aware OFDM receivers under time-varying conditions. In *2014 IEEE 8th Sensor Array and Multichannel Signal Processing Workshop (SAM)*, pages 341–344, 2014.

[12] J. Rodríguez-Piñeiro, M. Lerch, J. A. García-Naya, S. Caban, M. Rupp, and L. Castedo. Emulating extreme velocities of mobile LTE receivers in the downlink. *EURASIP Journal on Wireless Communications and Networking*, 2015, 2015.

[13] J. Rodriguez-Pineiro, P. Suarez-Casal, M. Lerch, S. Caban, J. A. Garcia-Naya, L. Castedo, and M. Rupp. LTE downlink performance in high speed trains. In *2015 IEEE 81st Vehicular Technology Conference (VTC Spring)*, pages 1–5, 2015.

[14] M. Lerch, J. Rodriguez-Pineiro, J. A. Garcia-Naya, and L. Castedo. Methods to perform high velocity LTE experiments at low velocities. In *2016 IEEE 83rd Vehicular Technology Conference (VTC Spring)*, pages 1–5, 2016.

[15] R. W. Chang. Synthesis of band-limited orthogonal signals for multichannel data transmission. *The Bell System Technical Journal*, 45(10):1775–1796, 1966.

[16] Erich Zöchmann, Stefan Pratschner, Stefan Schwarz, and Markus Rupp. Limited feedback in OFDM systems for combating ISI/ICI caused by insufficient cyclic prefix length. In *2014 48th Asilomar Conference on Signals, Systems and Computers*, pages 988–992, 2014.

[17] O. Edfors, M. Sandell, J. van de Beek, D. Landström, and F. Sjöberg. volume TULEA 1996:16. Luleå University of Technology, 1996.

[18] JG Proakis and DG Manolakm. Digital signal processing, second edizion, 1992.

[19] Stefan Pratschner, Bashar Tahir, Ljiljana Marijanovic, Mariam Mussbah, Kiril Kirev, Ronald Nissel, Stefan Schwarz, and Markus Rupp. Versatile mobile communications simulation: the Vienna 5G Link Level Simulator. *EURASIP Journal on Wireless Communications and Networking*, 2018(1):226, September 2018.

[20] Stefan Pratschner, Martin Klaus Müller, Fjolla Ademaj, Armand Nabavi, Bashar Tahir, Stefan Schwarz, and Markus Ruppy. Verification of the vienna 5G link and system level simulators and their interaction. In *2019 16th IEEE Annual Consumer Communications Networking Conference (CCNC)*, pages 1–8, 2019.

[21] Vahid Tarokh and Hamid Jafarkhani. On the computation and reduction of the peak-to-average power ratio in multicarrier communications. *IEEE Transactions on Communications*, 48(1):37–44, 2000.

Die approbierte gedruckte Originalversion dieser Diplomarbeit ist an der TU Wien Bibliothek verfügbar
The approved original version of this thesis is available in print at TU Wien Bibliothek.
TU Bibliothek Your knowledge hub WIEN

[22] Richard DJ Van Nee and Ramjee Prasad. OFDM for wireless multimedia communications. 2000.

[23] JG Proakis. Digital communications 4th ed. mcgraw-hill. *New York*, 2001.

[24] Hideki Ochiai and Hideki Imai. On clipping for peak power reduction of OFDM signals. In *Globecom'00-IEEE. Global Telecommunications Conference. Conference Record (Cat. No. 00CH37137)*, volume 2, pages 731–735. IEEE, 2000.

[25] Jean Armstrong. Peak-to-average power reduction for OFDM by repeated clipping and frequency domain filtering. *Electronics letters*, 38(5):246–247, 2002.

[26] Rorie O'Neill and Luis B Lopes. Envelope variations and spectral splatter in clipped multicarrier signals. In *Proceedings of 6th International Symposium on Personal, Indoor and Mobile Radio Communications*, volume 1, pages 71–75. IEEE, 1995.

[27] Xiaodong Li and Leonard J Cimini. Effects of clipping and filtering on the performance of OFDM. In *1997 IEEE 47th Vehicular Technology Conference. Technology in Motion*, volume 3, pages 1634–1638. IEEE, 1997.

[28] José Tellado and John M Cioffi. Peak power reduction for multicarrier transmission. In *IEEE GLOBECOM*, volume 99, pages 5–9, 1998.

[29] Jung-Chieh Chen and Chih-Peng Li. Tone reservation using near-optimal peak reduction tone set selection algorithm for PAPR reduction in OFDM systems. *IEEE Signal Processing Letters*, 17(11):933–936, 2010.

[30] Seung Hee Han and Jae Hong Lee. Papr reduction of OFDM signals using a reduced complexity PTS technique. *IEEE Signal Processing Letters*, 11(11):887–890, 2004.

[31] Jun Hou, Jianhua Ge, and Jing Li. Peak-to-average power ratio reduction of OFDM signals using PTS scheme with low computational complexity. *IEEE Transactions on Broadcasting*, 57(1):143–148, 2011.

[32] C. Tellambura. Improved phase factor computation for the PAR reduction of an OFDM signal using PTS. *IEEE Communications Letters*, 5(4):135–137, 2001.

[33] L.J. Cimini and N.R. Sollenberger. Peak-to-average power ratio reduction of an OFDM signal using partial transmit sequences. *IEEE Communications Letters*, 4(3):86–88, 2000.

[34] Stefan H Muller and Johannes B Huber. OFDM with reduced peak-to-average power ratio by optimum combination of partial transmit sequences. *Electronics letters*, 33(5):368–369, 1997.

Die approbierte gedruckte Originalversion dieser Diplomarbeit ist an der TU Wien Bibliothek verfügbar
The approved original version of this thesis is available in print at TU Wien Bibliothek.
TU Bibliothek Your knowledge hub WIEN

[35] Wong Sai Ho, AS Madhukumar, and Francois Chin. Peak-to-average power reduction using partial transmit sequences: a suboptimal approach based on dual layered phase sequencing. *IEEE transactions on broadcasting*, 49(2):225–231, 2003.

[36] Robert W Bauml, Robert FH Fischer, and Johannes B Huber. Reducing the peak-to-average power ratio of multicarrier modulation by selected mapping. *Electronics letters*, 32(22):2056–2057, 1996.

[37] H Breiling, Stefan H Muller-Weinfurtner, and Johannes B Huber. SLM peak-power reduction without explicit side information. *IEEE Communications Letters*, 5(6):239–241, 2001.

[38] Stéphane Y Le Goff, Samer S Al-Samahi, Boon Kien Khoo, Charalampos C Tsimenidis, and Bayan S Sharif. Selected mapping without side information for papr reduction in OFDM. *IEEE Transactions on Wireless Communications*, 8(7):3320–3325, 2009.

[39] Chin-Liang Wang and Yuan Ouyang. Low-complexity selected mapping schemes for peak-to-average power ratio reduction in OFDM systems. *IEEE Transactions on signal processing*, 53(12):4652–4660, 2005.

[40] Chih-Peng Li, Sen-Hung Wang, and Chin-Liang Wang. Novel low-complexity SLM schemes for PAPR reduction in OFDM systems. *IEEE Transactions on Signal Processing*, 58(5):2916–2921, 2010.

[41] P Van Eetvelt, G Wade, and M Tomlinson. Peak to average power reduction for OFDM schemes by selective scrambling. *Electronics letters*, 32(21):1963–1964, 1996.

[42] ADSJ TELLAMBURA. C. reducing the peak-to-average power ratio of orthogonal frequency division multiplexing signal through bit or symbol interleaving. *Electronics Letters*, 36(13):1161–1163, 2000.

[43] Anagiyaddage DS Jayalath and Chintha Tellambura. Reducing the peak-to-average power ratio of an OFDM signal by interleaving. In *conference;*, 2000.

[44] A Dhammika S Jayalath and Chintha Tellambura. The use of interleaving to reduce the peak-to-average power ratio of an OFDM signal. In *Globecom'00-IEEE. Global Telecommunications Conference. Conference Record (Cat. No. 00CH37137)*, volume 1, pages 82–86. IEEE, 2000.

Die approbierte gedruckte Originalversion dieser Diplomarbeit ist an der TU Wien Bibliothek verfügbar
The approved original version of this thesis is available in print at TU Wien Bibliothek.
TU Bibliothek Your knowledge hub WIEN

[45] Seung Hee Han and Jae Hong Lee. An overview of peak-to-average power ratio reduction techniques for multicarrier transmission. *IEEE Wireless Communications*, 12(2):56–65, 2005.

[46] Yasir Rahmatallah and Seshadri Mohan. Peak-to-average power ratio reduction in OFDM systems: A survey and taxonomy. *IEEE Communications Surveys Tutorials*, 15(4):1567–1592, 2013.

[47] Tao Jiang and Yiyan Wu. An overview: Peak-to-average power ratio reduction techniques for OFDM signals. *IEEE Transactions on Broadcasting*, 54(2):257–268, 2008.

[48] H. Bogucka, A. Kliks, and P. Kryszkiewicz. *Filter-Bank-Based Multicarrier Technologies*, pages 193–218. 2016.

[49] B. Saltzberg. Performance of an efficient parallel data transmission system. *IEEE Transactions on Communication Technology*, 15(6):805–811, 1967.

[50] B. Farhang-Boroujeny and C. H. Yuen. Cosine modulated and offset QAM filter bank multicarrier techniques: A continuous-time prospect. In *EURASIP Journal on Advances in Signal Processing*, 2010.

[51] Frank Schaich and Thorsten Wild. Waveform contenders for 5G — OFDM vs. FBMC vs. UFMC. In *2014 6th International Symposium on Communications, Control and Signal Processing (ISCCSP)*, pages 457–460, 2014.

[52] F. L. Luo and C. Zhang. *From OFDM to FBMC: Principles and Comparisons*, pages 47–66. 2016.

[53] Maurice Bellanger, D Le Ruyet, D Roviras, M Terré, J Nossek, L Baltar, Q Bai, D Waldhauser, M Renfors, T Ihalainen, et al. FBMC physical layer: a primer. *Phydyas*, 25(4):7–10, 2010.

[54] Ralf Haas and Jean-Claude Belfiore. A time-frequency well-localized pulse for multiple carrier transmission. *Wireless personal communications*, 5(1):1–18, 1997.

[55] Ronald Nissel and Markus Rupp. On pilot-symbol aided channel estimation in FBMC-OQAM. In *2016 IEEE international conference on acoustics, speech and signal processing (ICASSP)*, pages 3681–3685. IEEE, 2016.

[56] R. Nissel, S. Schwarz, and M. Rupp. Filter bank multicarrier modulation schemes for future mobile communications. *IEEE Journal on Selected Areas in Communications*, 35(8):1768–1782, 2017.

Die approbierte gedruckte Originalversion dieser Diplomarbeit ist an der TU Wien Bibliothek verfügbar
The approved original version of this thesis is available in print at TU Wien Bibliothek.
TU Bibliothek Your knowledge hub WIEN

[57] Ronald Nissel. *Filter bank multicarrier modulation for future wireless systems*. PhD thesis, Wien, 2017.

[58] Ronald Nissel, Sebastian Caban, and Markus Rupp. Experimental evaluation of FBMC-OQAM channel estimation based on multiple auxiliary symbols. In *2016 IEEE Sensor Array and Multichannel Signal Processing Workshop (SAM)*, pages 1–5, 2016.

[59] Gerhard Wunder, Peter Jung, Martin Kasparick, Thorsten Wild, Frank Schaich, Yejian Chen, Stephan Ten Brink, Ivan Gaspar, Nicola Michailow, Andreas Festag, Luciano Mendes, Nicolas Cassiau, Dimitri Ktenas, Marcin Dryjanski, Slawomir Pietrzyk, Bertalan Eged, Peter Vago, and Frank Wiedmann. 5GNOW: non-orthogonal, asynchronous waveforms for future mobile applications. *IEEE Communications Magazine*, 52(2):97–105, 2014.

[60] Gerhard Wunder, Martin Kasparick, Stephan ten Brink, Frank Schaich, Thorsten Wild, Ivan Gaspar, Eckhard Ohlmer, Stefan Krone, Nicola Michailow, Ainoa Navarro, Gerhard Fettweis, Dimitri Ktenas, Vincent Berg, Marcin Dryjanski, Slawomir Pietrzyk, and Bertalan Eged. 5GNOW: Challenging the LTE design paradigms of orthogonality and synchronicity. In *2013 IEEE 77th Vehicular Technology Conference (VTC Spring)*, pages 1–5, 2013.

[61] Frank Schaich, Thorsten Wild, and Yejian Chen. Waveform contenders for 5G - suitability for short packet and low latency transmissions. In *2014 IEEE 79th Vehicular Technology Conference (VTC Spring)*, pages 1–5, 2014.

[62] Grigory Bochechka, Valery Tikhvinskiy, Ivan Vorozhishchev, Altay Aitmagambetov, and Bolat Nurgozhin. Comparative analysis of UFMC technology in 5G networks. In *2017 International Siberian Conference on Control and Communications (SIBCON)*, pages 1–6, 2017.

[63] Christoph Rapp. Effects of HPA-nonlinearity on a 4-DPSK/OFDM-signal for a digital sound broadcasting signal. *ESA Special Publication*, 332:179–184, 1991.

Die approbierte gedruckte Originalversion dieser Diplomarbeit ist an der TU Wien Bibliothek verfügbar
The approved original version of this thesis is available in print at TU Wien Bibliothek.
TU Bibliothek Your knowledge hub WIEN